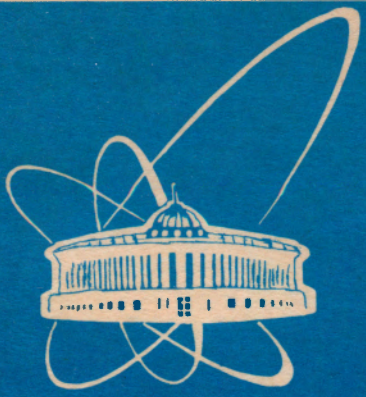

сообщения
объединенного
института
ядерных
исследований
дубна

E1-94-519

ELECTROPRODUCTION OF CHARGED PIONS FROM ^{1}H, ^{2}H, ^{40}Ca, AND ^{208}Pb

1994

N.N.Badalian, R.G.Badalian, M.Ya.Chubarian, A.A.Kuznetsov, V.N.Pechenov, Yu.A.Troyan, V.V.Uzhinskii
Joint Institute for Nuclear Research, 141980, Moscow Region, Russia

O.K.Baker, K.B.Beard, W.W.Buck, T.Eden, R.Madey
Center for Nuclear and High Energy Physics, Hampton University, Hampton, VA 23668, USA

J.Gomez, S.Nanda, A.Saha
Continuous Electron Beam Accelerator Facility, Newport News, VA 23606, USA

B.D.Anderson, D.Keane, A.Lai, D.M.Manley, J.W.Watson, W.-M.Zhang
Department of Physics Kent State University, Kent, OH 44242-0001, USA

J.Napolitano
Department of Physics Rensselaer Polytechnic Institute, Troy, NY 12180-3590, USA

1. Introduction

Duality between hadronic and quark–gluonic degrees of freedom in intermediate energy strong interaction physics is, and up to now, an unanswered principle in the area of modern particle physics. On the one hand, for $Q^2 \leq (1-2)$ $(\mathrm{GeV}/c)^2$ where Q^2 is the squared four–momentum transfer, the statistical properties of hadrons and interactions between hadrons can be described by hadronic degrees of freedom (*e.g.*, π–meson exchange diagrams, s and t channel resonance exchanges, *etc.*) as well as by the quark–parton representation, and by quark to hadron fragmentation functions. On the other hand, for the same region in Q^2, quark–gluonic degrees of freedom and perturbative–QCD (pQCD) descriptions of hadrons start to become important. In this transition region, where $Q^2 \simeq (1-2)$ $(\mathrm{GeV}/c)^2$, the descriptive power of hadronic degrees of freedom is decreasing; while at the same time, the importance of the quark–gluonic sector is on the rise — up to full domination in the region $Q^2 \geq (2-3)$ $(\mathrm{GeV}/c)^2$. Here lies the interest in studying this transition region from the point of view of strong–interaction dynamics.

In the so–called transition region, as we think, arise non–pQCD interactions between hadrons. These interactions find there realizations in phenomenological models, such as quark hadronization and nuclear color transparency, with respect to hadrons produced at high Q^2. For instance, the study of the space–time evolution of hadronic final states in deep–inelastic scattering is an interesting, yet at the same time, fundamental subject. The principal question is when quarks are struck by leptons or other currents, one would anticipate to observe the quarks in the final state; however, only ordinary hadrons emerge. Investigating the detail of the space–time evolution of the hadronization process in electroproduction, the time when the quark is hit to the time when the final hadrons appear as asymptotic states, one should learn something about the dynamics of confinement. Many models, such as the parton model, have been employed to understand the dynamics of hadronization. We discuss this concept, in detail, in a later section of this proposal. Here we would like only to emphasize the close relationship between the transition region and the phenomena of quark hadronization along with nuclear color transparency.

In this document, we propose to investigate the decreasing mechanism of the hadronic component (Δ, ρ, *etc.*) simultaneously with the increasing quark–gluonic component from the inclusive electroproduction of charged pions in the transition region $1.0 \leq Q^2$ $(\mathrm{GeV}/c)^2 \leq 2.5$ and $W \geq 2.0$ GeV. From this study (amongst other things), we hope to understand the space–time evolution of quark hadronization via a Q^2–analysis of nuclear transparency through the inclusive $(e, e'\pi^+)$ reaction on ^{2}H, ^{40}Ca, and ^{208}Pb nuclei. We also plan to determine the contribution from Δ and ρ hadronic resonances to the inclusive spectra of electroproduced pions, and investigate the electroproduced pion charge asymmetry $\eta(z, Q^2)$ from the proton data (see Section III for further details). Lastly, to acquire knowledge about these topics, will give us a deeper understanding of nonperturbative–QCD dynamics.

The format of the proposal is as follows: Sections II.1.1–3 cover the theoretical development of various inclusive pion electroproduction channels that we employ to set properly the physics content in our proposal. The rest of Section II.1 deals with prior experiments performed at DESY: positive and negative hadrons produced from inelastic e–p scattering at incident electron energies of 7.2 GeV. Section II.2.1 discusses various theoretical developments concerning nuclear color transparency and interactions of produced pions traversing the nuclear medium. Section II.2.2 canvasses several models that interpret the phenomenology of quark hadronization. The rest of Section II.2 deals with the rescattering of pions produced as they cross the nuclear

medium and the few experiments that have studied the inclusive leptoproduction of hadrons in atomic nuclei. Section III details the goals of our experiment, expected background processes, multiple scattering of pions, and expected real event count rates, and some insight into the nuclear transparency off-line analysis of the data. Lastly, because this experiment was initially submitted to PAC 7 as a letter of intent, we discuss the observations made by the PAC and the eventual modifications done to our proposal.

2. Physics Motivation

2.1 Pion Electroproduction from Protons and Deuterium

2.1.1 Process $ep \to e'\pi^+n$: Formalism and Theoretical Models

At fixed electron scattering kinematics, the maximum momentum of electroproduced π^+–mesons along the direction of the three–momentum transfer is from the direct reaction $ep \to e'\pi^+n$. From the point of view of Feynman diagrams, this reaction is the simplest π^+–meson production process. The π^+–meson electroproduction cross–section can be related to the pion photoproduction cross section via the relation [1, 2, 3, 4, 5, 6]

$$\frac{d^5\sigma}{d\Omega_e dE_e d\Omega_\pi}(ep \to e'\pi^+n) = \Gamma \frac{d^2\sigma}{d\Omega_\pi}(\gamma^V p \to \pi^+ n) \ , \tag{1}$$

where

$$\Gamma = \frac{\alpha}{2\pi^2 Q^2} \frac{E_e}{E_{beam}} \frac{K}{1-\varepsilon} \ , \tag{2}$$

and K is given by

$$K = (W^2 - m_p^2)/2m_p^2 \ . \tag{3}$$

Here W is the invariant mass of the final hadronic system, m_p is the proton mass, and the fine structure constant is $\alpha = 1/137.036$. The polarization parameter ε is defined by

$$\frac{1}{\varepsilon} = 1 + 2\left(1 + \frac{\nu^2}{Q^2}\right)\tan^2\left(\frac{\theta_e}{2}\right) \ , \tag{4}$$

where $\nu = E_{beam} - E_e$ is the energy transfer and θ_e is the electron scattering angle. In general, the cross section $d^2\sigma/d\Omega_\pi$ is given by:

$$\frac{d^2\sigma}{d\Omega_\pi} = \frac{d^2\sigma_T}{d\Omega_\pi} + \varepsilon\frac{d^2\sigma_L}{d\Omega_\pi} + \varepsilon\frac{d^2\sigma_{TT}}{d\Omega_\pi}\cos(2\varphi) + \sqrt{\frac{\varepsilon(1+\varepsilon)}{2}}\frac{d^2\sigma_{TL}}{d\Omega_\pi}\cos(\varphi) \ . \tag{5}$$

Here φ is the angle between the electron scattering plane and the pion production plane, $d^2\sigma_T/d\Omega_\pi$ is the transverse cross–section, $d^2\sigma_L/d\Omega_\pi$ is the longitudinal cross–section, $d^2\sigma_{TT}/d\Omega_\pi$ is the cross–section originating from the interference between the transverse components of the virtual photon and $d^2\sigma_{LT}/d\Omega_\pi$ is the cross section arising from the interference between the transverse and longitudinal polarizations of the virtual photon.

In the framework of the Born approximation, four diagrams are used to describe the reaction components of $d^2\sigma/d\Omega_\pi$. These are the s, t, and u–channel exchange diagrams along with the

contact terms for the vertex $\gamma^V p\pi^+ n$. The expressions for the cross sections $d^2\sigma_J/d\Omega_\pi$ where $J = T, L, TT, TL$ can be found in Refs.[1, 2, 3]. Here we present only the longitudinal component of the cross section in the Born approximation, because for small t, the longitudinal cross section is the main contributor to the pion production cross section

$$\frac{d^2\sigma_L}{d\Omega_\pi} \simeq \frac{Q^2}{q^2}\frac{P_\pi}{q}[F_7^2 + F_8^2 + 2\cos\vartheta_\pi F_7 F_8] \ . \tag{6}$$

Where the values F_7 and F_8 are given by:

$$F_7 = C_7\left[(W+m_p)\frac{F_{1p}(Q^2)}{W^2-m_p^2} - (2E_\pi - q_0)\frac{F_\pi(Q^2)}{t-m_\pi^2} + q_0\frac{F_\pi(Q^2) - F_{1p}(Q^2)}{Q^2}\right] \ , \tag{7}$$

and

$$F_8 = -C_8\left[(W-m_p)\frac{F_{1p}(Q^2)}{W^2-m_p^2} - (2E_\pi - q_0)\frac{F_\pi(Q^2)}{t-m_\pi^2} + q_0\frac{F_\pi(Q^2) - F_{1p}(Q^2)}{Q^2}\right] \ . \tag{8}$$

where $C_7 = \sqrt{(E_1+m_p)(E_2-m_p)}$ and $C_8 = \sqrt{(E_1-m_p)(E_2+m_p)}$. We would like to note that all non–invariant kinematic variables in Eqs. (5) – (8) and below in this subsection, are with respect to the $(\gamma^V p)$ center–of–mass system. E_1 and E_2 are the energy of the proton before and after interaction, respectively, q_0 and $q = |\vec{q}|$ are the energy and momentum of the virtual photon, respectively.

In the Born approximation, the interference cross sections $d^2\sigma_{TT}/d\Omega_\pi$ and $d^2\sigma_{TL}/d\Omega_\pi$ are approximately given by the following relations

$$\frac{d^2\sigma_{TT}}{d\Omega_\pi} \sim \sin^2\vartheta_\pi \tag{9}$$

$$\frac{d^2\sigma_{TL}}{d\Omega_\pi} \sim \sin\vartheta_\pi \ , \tag{10}$$

and are small in comparison to the other Born terms with respect to the direction of the virtual photon three momentum.

The results of the calculation for the cross–section terms $d^2\sigma_L/d\Omega_\pi$ and $d^2\sigma_T/d\Omega_\pi$ in the framework of the Born approximation are displayed in Fig. 1. For the pion charge form factor $F_\pi(Q^2)$, we used the expression [7, 8, 4, 5]

$$F_\pi(Q^2) = \frac{1}{1+Q^2/m_\rho^2} \ , \tag{11}$$

where m_ρ is the ρ–meson mass.

Further improvement to the Born Approximation by treating the nucleon form factors as free parameters (perhaps justified by the fact that the nucleon is far off its mass shell whereas the pion is near to its pole) was undertaken by Gutbrod and Kramer [3]. Improvement was seen between the theoretical prediction of the Born Approximation and the experimental [5]. For the nucleon case, the form factor value is about 50% above their on–mass shell values. The comparison between the Born Approximation and its modifications [1, 2, 3] with the data are presented in Refs. [7, 8, 4, 5, 9, 6].

In this proposal, we use the modified Born Approximation [3] in simulating the process $ep \to e'\pi^+n$.

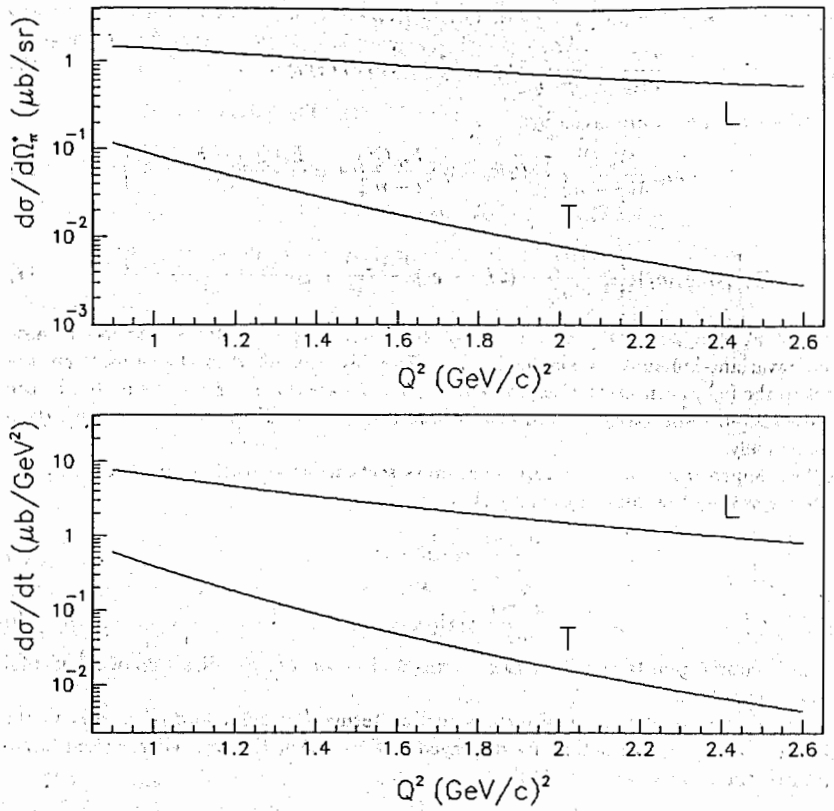

Fig. 1 The Q^2 dependence of the longitudinal (L) and transverse (T) components of the Born cross section for the $ep \to e'\pi^+ n$ process at $x_B = 0.3$. The $d^2\sigma/d\Omega^*_\pi$ – cross-section in the $(\pi^+ n)$ center of mass system.

2.1.2 Process $ep \to e'\pi^+\pi^- p$: Formalism and Theoretical Models

Cross sections for Δ^{++}, Δ^0, and ρ^0 production from the reaction $ep \to e'\pi^+\pi^- p$ were determined Refs. [10, 11] by a maximum likelihood fit to the Dalitz density plot $dN(M^2_{p\pi^+}, M^2_{\pi^+\pi^-})$

$$dN(M^2_{p\pi^+}, M^2_{\pi^+\pi^-}) = \Big[a_{\Delta^{++}} F_{\Delta^{++}}(M_{p\pi^+}) W_\Delta(\cos\vartheta_{H\Delta}) + a_{\Delta^0} F_{\Delta^0}(M_{p\pi^-}) + a_\rho F_\rho(M_{\pi^+\pi^-}) W_\rho(\cos\vartheta_{H\rho}) + a_{PS} F_{PS}\Big] dM^2_{p\pi^+} dM^2_{\pi^+\pi^-} \quad , \tag{12}$$

where the quantities $a_{\Delta^{++}}$, a_{Δ^0}, a_ρ, and a_{PS} are fit parameters and gauge the size of the $ep \to e'\pi^-\Delta^{++}$, $ep \to e'\pi^+\Delta^0$, $ep \to e'\rho^0 p$ channels and phase space like background contributions, respectively; F_{PS} is a constant which describes events distributed uniformly over the Dalitz plot and is normalized to the ρ and Δ contributions. F_Δ and F_ρ describe normalized Breit–Wigner distributions, *e.g.*, for the ρ-meson we have $F_\rho = B_\rho / I_\rho$ with

$$B_\rho = \frac{M_{\pi^+\pi^-}}{q M_{\pi^+\pi^-}} \frac{\Gamma(M_{\pi^+\pi^-})}{\left(M^2_\rho - M^2_{\pi^+\pi^-}\right)^2 + M^2_\rho \Gamma^2(M_{\pi^+\pi^-})} \tag{13}$$

Here M is the $\pi^+\pi^-$ effective mass and $\Gamma(m) = \Gamma_\rho (q/q_0)(m_\rho/m) U_1(qr)/U_1(q_0 r)$; q and q_0 are the π momenta in the $\pi^+\pi^-$ rest frame at the mass m and m_ρ, respectively; $r = 2.2$ GeV^{-1} and

$$U_1(x) = \frac{x^2}{2}\left[\frac{2x^2+1}{4x^2}\ln(4x^2+1) - 1\right] \quad . \tag{14}$$

The normalization constant I_ρ is obtained for a given event from an integration over the Dalitz plot

$$I_\rho = \int B_\rho W_\rho dM^2_{p\pi^+} dM^2_{\pi^+\pi^-} \quad . \tag{15}$$

$W_\rho(\cos\vartheta_{H\rho})$ describes the ρ polar decay angular distribution in the helicity frame and is given by

$$W_\rho(\cos\vartheta_{H\rho}) = \frac{3}{4}\left[1 + r^{04}_{33} + (1 - 3r^{04}_{33})\right]\cos^2\vartheta_{H\rho} \quad , \tag{16}$$

where $\vartheta_{H\rho}$ is the polar decay angle for the produced ρ with respect to the line of flight of the ρ and the density matrix element r^{04}_{33} lies between 0 and 0.5. $W_\Delta(\cos\vartheta_{H\Delta})$ is the corresponding distribution for Δ decay [11].

The measurements with the Hall A HRS2 system, one spectrometer will be used to detect and measure the angle and momentum of the the scattered electron, and the other will measure the momentum and angle of the produced hadron (*i.e.*, the π^-–meson). In this case, the channel $\pi^+\pi^- p$ can be selected from the off–line analysis by the missing–mass condition $M_x = M_{\pi^+ p} < (m_p + 2m_\pi)$, where m_π is the mass of the pion. We plan to analyze the obtained data by the expression:

$$\frac{d^3\sigma}{d\Omega_\pi dP_\pi}(\gamma^V p \to \pi^\pm X) = a_{\Delta^{++}} \int_{M^{min}_{p\pi^+}}^{M^{max}_{p\pi^+}} F_{\Delta^{++}}(M_{p\pi^+})dM_{p\pi^+} + a_{\Delta^0} \int_{M^{min}_{p\pi^-}}^{M^{max}_{p\pi^-}} F_{\Delta^0}(M_{p\pi^-})dM_{p\pi^-} +$$

$$a_\rho \int_{M^{min}_{\pi^+\pi^-}}^{M^{max}_{\pi^+\pi^-}} F_\rho(M_{\pi^+\pi^-})dM_{\pi^+\pi^-} + a_{deep}\frac{d^3\sigma}{d\Omega_\pi dP_\pi}(\gamma^V p \to \pi^\pm X) \quad (17)$$

The cross sections for Δ^{++}, Δ^0, and ρ production will be determined by the maximum likelihood fit to the expressions given in Eqs. (12) and (17). The maximal and minimal values of the quantities $M_{p\pi^+}$, $M_{p\pi^-}$ and $M_{\pi^+\pi^-}$ are defined from Dalitz plot analyses.

Simulation results using Eqs. (12) and (17) for the reactions $\gamma^V p \to \pi^+\pi^- p$, $\gamma^V p \to \pi^+ X$ and $\gamma^V d \to \pi^+ X$ are presented in Figs. 2 and 3. For the case of π^+–meson production, the contribution from the $\gamma^V p \to \pi^+ n$ channel are taken into account within the framework of the modified Born Approximation. The deep–inelastic contribution, which is given by the last term in Eq. (17), will be discussed in the next subsection.

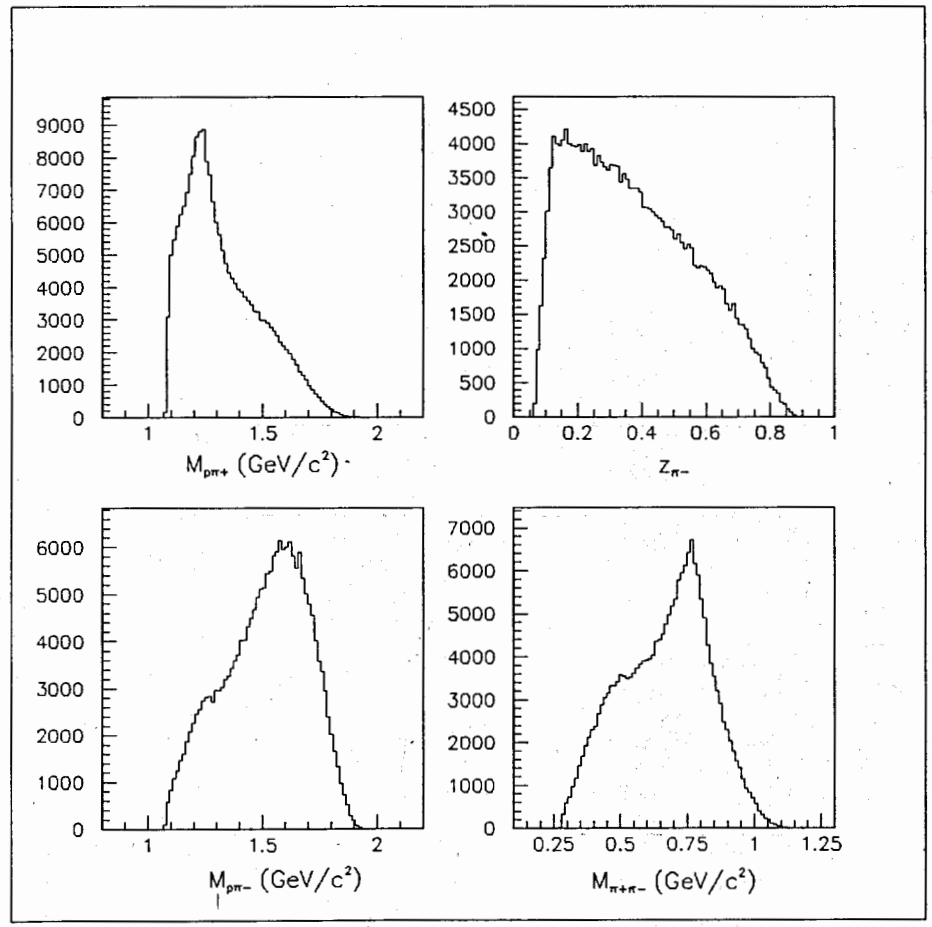

Fig. 2 Effective masses distributions $M_{p\pi^+}$, $M_{p\pi^-}$, $M_{\pi^+\pi^-}$ and z_{π^-} distribution from the reaction $\gamma^V p \to \pi^+\pi^- p$ at $Q^2 \simeq 1.2$ (GeV/c)^2 and $W \simeq 1.9$ GeV with a 4π acceptance for hadrons. The parameter values $a_{\Delta^{++}}$, a_{Δ^0}, a_ρ and a_{PS} are given in Table 4.

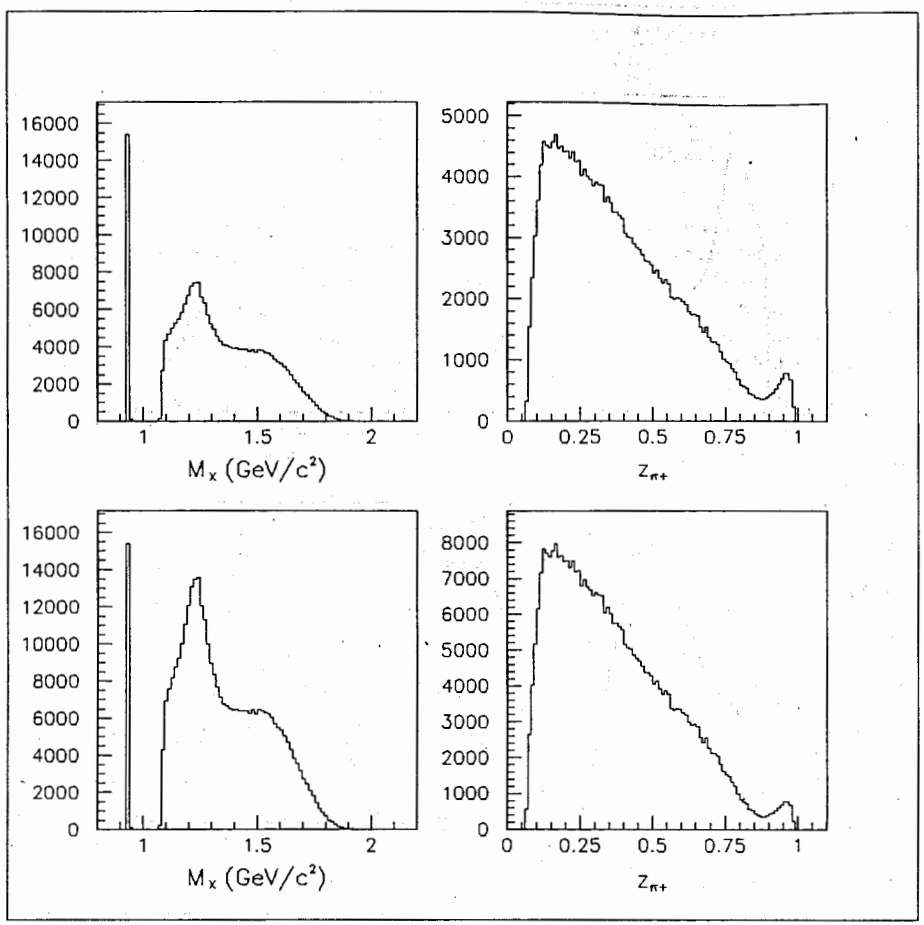

Fig. 3 Missing mass M_x and $z_{\pi+}$ distributions from the reaction $\gamma^V p \to \pi^+ X$ (up histograms) and $\gamma^V D \to \pi^+ X$ (down histograms) at $Q^2 \simeq 1.2$ (GeV/c)^2 and $W \simeq 1.9$ GeV with a 4π acceptance for hadrons. For the deuterium case, we made a shift on the nucleon mass to make the M_x distribution.

2.1.3 Process $ep \to e'\pi^{\pm}X$: Formalism and Theoretical Models

The general inclusive hadron electroproduction cross section is given by [12, 13, 14, 15]

$$\frac{d^6\sigma}{d\Omega_e dE_e d\Omega_\pi dP_\pi}(ep \to e'\pi^{\pm}X) = \Gamma \frac{d^3\sigma}{d\Omega_\pi dP_\pi}(\gamma^V p \to \pi^{\pm}X) \ , \tag{18}$$

where Γ represents the usual virtual photon flux. The invariant cross section for pion electroproduction is usually given in terms of the quark to hadron fragmentation function $D(z)$ [13, 12, 16, 17]:

$$E_\pi \frac{d^3\sigma}{d\vec{P}_\pi}(ep \to e'\pi^{\pm}X) = \sigma_{tot}(Q^2,\nu) z F_p^{\pi^{\pm}}(x_B, z) B \exp(-BP_T^2) \ , \tag{19}$$

where $\sigma_{tot}(Q^2,\nu)$ is the total virtual photon-proton cross section, $z = E_h/\nu$, P_T is the transverse momentum of the pion, and $B = 4.37 \pm 0.21$ (GeV/c)^2 [12].

The total virtual-photon absorption cross section $\sigma_{tot}(Q^2,\nu)$ related to the inclusive spectra of the scattered electron is given by

$$\frac{d^3\sigma}{dE_e d\Omega_e}(ep \to e'X) = \Gamma\, \sigma_{tot}(Q^2,\nu) = \Gamma\, \left[\sigma_T(Q^2,\nu) + \varepsilon\sigma_L(Q^2,\nu)\right] \tag{20}$$

where $\sigma_T(Q^2,\nu)$ and $\sigma_L(Q^2,\nu)$ are the transverse and longitudinal photon absorption cross sections by the proton, respectively. These cross sections are related to the proton structure functions $W_1(Q^2,\nu)$ and $W_2(Q^2,\nu)$ by

$$\sigma_T(Q^2,\nu) = \frac{4\pi^2\alpha}{K} W_1(Q^2,\nu) \tag{21}$$

$$\sigma_L(Q^2,\nu) = \frac{4\pi^2\alpha}{K} \left[\left(1 + \frac{\nu^2}{Q^2}\right) W_2(Q^2,\nu) - W_1(Q^2,\nu)\right] \ , \tag{22}$$

where $K = (W^2 - m_p^2)/2m_p^2$ as in Eq. (2). For the empirical parametrization of the nucleon structure functions, the available W region is divided into three parts [18]: the quasielastic scattering region $W \simeq m_p$ [19], the resonance region $W < 1.8$ GeV [20], and the inelastic scattering region $W > 2.0$ GeV [21]. Because the kinematic region for the proposed experiment is at $W > 1.9$ GeV, we use the Rittenberg-Rubinstein parametrization for the proton structure functions [21, 18] in simulating the channels $ep \to e'\pi^{\pm}X$

$$2m_p W_1(Q^2,\nu) = F_1(\omega_1) \ , \tag{23}$$

$$\nu W_2(Q^2,\nu) = \frac{F_2(\omega_2)}{\omega_2} \ , \tag{24}$$

where (with $j = 1,\ 2$)

$$\omega_j = \frac{2m_p\nu + M_j^2}{Q^2 + a_j^2} \tag{25}$$

and

$$F_j(\omega_j) = \omega_j \sum_{n=3}^{7} b_n^{(j)} \left(1 + \frac{1}{\omega_j}\right)^n \ . \tag{26}$$

j	M_j^2 (GeV^2)	a_j^2 (GeV^2)	$b_3^{(j)}$	$b_4^{(j)}$	$b_5^{(j)}$	$b_6^{(j)}$	$b_7^{(j)}$
1	1.95 ± 0.06	0.37 ± 0.02	1.565	−8.995	30.74	−39.51	16.57
2	1.43 ± 0.06	0.42 ± 0.02	0.933	−1.494	9.021	−14.50	6.453

Table 1: The Rittenberg and Rubinstein parameters

The parameters M_j^2, a_j^2, and $b_n^{(j)}$ are presented in Table 1.

The function $F_p^{\pi^\pm}(x_B, z)$ in Eq. (19) and $F_n^{\pi^\pm}(x_B, z)$ are related to the quark distribution functions in the nucleon and the quark to hadron fragmentation functions by [22, 23, 24]

$$\frac{1}{\sigma_{tot}}\frac{d\sigma}{dz}(\gamma^V p \to \pi^\pm X) = F_p^{\pi^\pm}(x_B, z) = \frac{4\left[u(x_B)D_u^{\pi^\pm} + \overline{u}(x_B)D_u^{\pi^\mp}\right] + d(x_B)D_u^{\pi^\mp} + \overline{d}(x_B)D_u^{\pi^\pm} + s(x_B)D_u^{\pi^-} + \overline{s}(x_B)D_u^{\pi^-}}{4\left[u(x_B) + \overline{u}(x_B)\right] + d(x_B) + \overline{d}(x_B) + s(x_B) + \overline{s}(x_B)} \quad (27)$$

$$\frac{1}{\sigma_{tot}}\frac{d\sigma}{dz}(\gamma^V n \to \pi^\pm X) = F_n^{\pi^\pm}(x_B, z) = \frac{4\left[d(x_B)D_u^{\pi^\pm} + \overline{d}(x_B)D_u^{\pi^\mp}\right] + u(x_B)D_u^{\pi^\mp} + \overline{u}(x_B)D_u^{\pi^\pm} + s(x_B)D_u^{\pi^-} + \overline{s}(x_B)D_u^{\pi^-}}{4\left[d(x_B) + \overline{d}(x_B)\right] + u(x_B) + \overline{u}(x_B) + s(x_B) + \overline{s}(x_B)} \quad (28)$$

An analysis was performed in Ref.[17] to investigate the up and down quark to charged–pion fragmentation functions using data that was obtained at BEBC [25]. The results of this analysis [17] are presented in Fig. 4 and were used in our simulation of the deep–inelastic contribution to the inclusive spectra of $\pi^\pm$–mesons.

Another analysis that will be performed for this channel is the dependence of the electroproduced charge asymmetry $\eta(z, Q^2)$ on Q^2 and z

$$\eta(z, Q^2) = \frac{N_{\pi^+} - N_{\pi^-}}{N_{\pi^+} + N_{\pi^-}} \,. \quad (29)$$

The value of the charge asymmetry η for real photons is $\sim (5 - 10)\%$ [26, 27], where η is apparently being connected to annihilation–type diagrams. As already mentioned, in the nucleon's rest system, the photon changes into a quark–antiquark pair; which in the case of real photons, interacts mainly with the nucleon through the exchange of a two gluon (multigluon) colorless state (pomeron). After interaction, the incoherent quark–gluon state, where the initial state quantum numbers are conserved, is fragmented into final–state hadrons. Such interaction and hadronization mechanisms are dominant for the case with real photons. The yield of fast hadrons with different isotopic composition (or charge) must be the same because the initial state, that is the photon's quark–gluon fluctuation, is neutral [*e.g.*, $d\sigma(\gamma p \to \pi^+ X) = d\sigma(\gamma p \to \pi^- X)$, *etc.*].

However, along with a two gluon (multigluon) or pomeron exchange, the photon–nucleon interaction may contribute also to an annihilation process of a component of the quark–antiquark

pair, from which the photon converted. In this case, only one quark (antiquark) can take part in the hadroproduction process (fast hadron production is meant); hence, there arises an asymmetry in the hadron yields of, say, π^+ and π^- mesons. The value of that asymmetry is entirely defined by the cross section of annihilation for the antiquark (quark) of the pair with the quark (antiquark) of the nucleon.

For the case of a virtual photon with $Q^2 > m_c^2$ [note that $(0.1 - 0.2) \leq m_c^2\ (\mathrm{GeV}/c)^2 \leq 0.5$], the interaction of the virtual photon with the quark (antiquark) of the nucleon which corresponds to annihilation of the slow antiquark (quark) of the pair in the laboratory system leads to an asymmetry in the yields of π^+ and π^- mesons. But this asymmetry is defined already by the isotopic composition of the target and is different for the proton and neutron. For example, for the proton, $N_{h^+}/N_{h^-} \simeq (2-3)$, which corresponds to $\eta(z, Q^2) \simeq (30-50)\%$ at $Q^2 \simeq 2\ (\mathrm{GeV}/c)^2$ and $z \simeq (0.8 - 0.9)$ [28, 29]. The expected z dependence of the charge asymmetry $\eta(z, Q^2)$ at $Q^2 \simeq 1.2\ (\mathrm{GeV}/c)^2$ are presented in Fig. 5.

In the transition region for Q^2 (*i.e.*, $0 < Q^2 < m_c^2$), $\pi^\pm$ mesons will contribute to the interaction through gluon exchange as well as for annihilation of one of the components of the quark–antiquark pair in the nucleon; hence, $\eta(z, Q^2)$ for fast pions ($z \geq 0.5$) will have a minimal value of $\sim (5 - 10)\%$ at $Q^2 \simeq 0$, and will grow at $Q^2 \gg m_c^2$ up to the maximum value possible at a given isotopic composition of the target, which in case of a proton is $\simeq (30 - 50)\%$. From the point of view of photon interactions with gluons and quarks, the experimental investigation of the charge asymmetry $\eta(z, Q^2)$ against Q^2, z and possibly on ν, is of considerable interest.

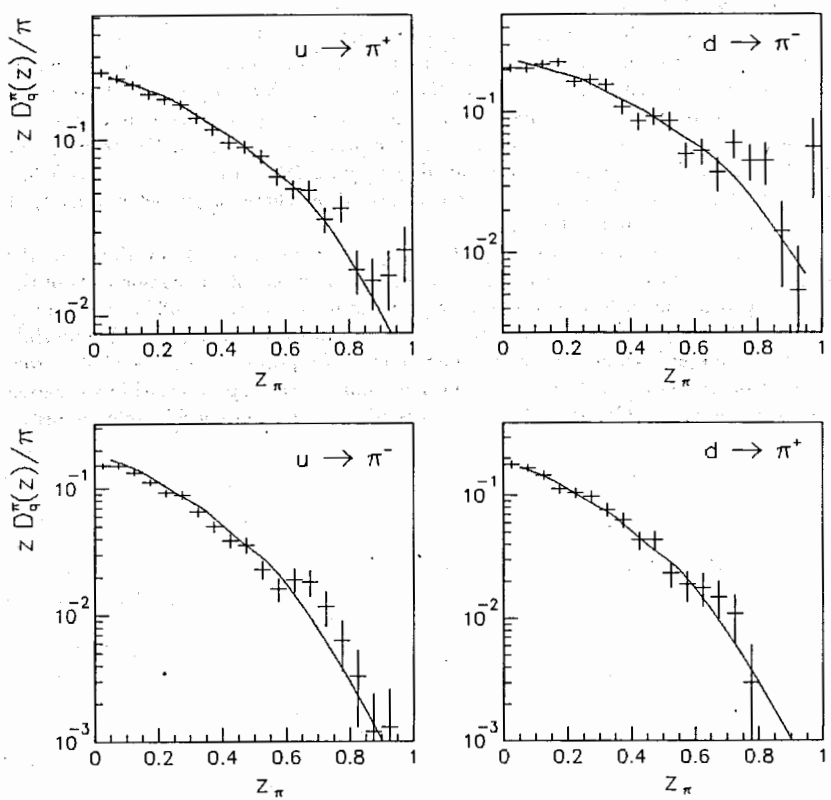

Fig. 4 Up quark to $\pi^{\pm}$ and down quark to $\pi^{\pm}$ fragmentation functions. Experimental points are from [25]. See text for explanation of the curves.

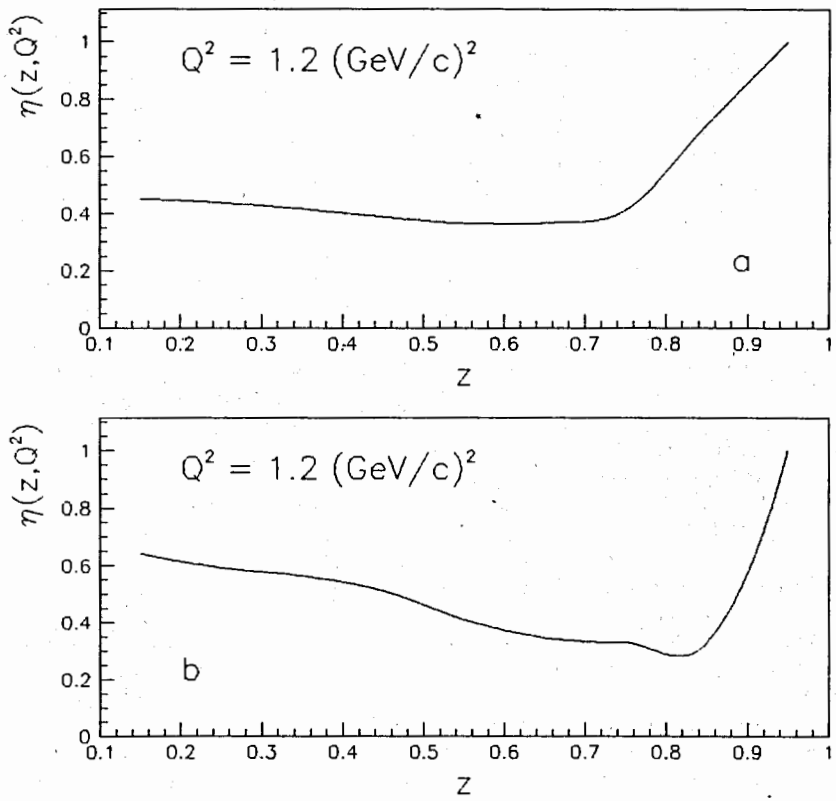

Fig. 5 The charge asymmetry $\eta(z, Q^2)$ vs. z at $Q^2 \simeq 1.2$ (GeV/c)^2 and $x_B = 0.3$ for a 4π acceptance for hadrons (top), and for setup **1** for the proposed experiment (bottom).

2.1.4 Prior Experiments

In this subsection we would like to concentrate on pion electroproduction with pion multiplicity greater than one because in the case of $\gamma^V p \to \pi^+ n$ most experimental studies are related to pion form factor measurements and for testing of the Born Approximation model.

Detailed studies of positive and negative hadrons produced from inelastic e–p scattering at incident electron energies of 7.2 GeV are presented in Refs.[10, 30, 31, 14, 11]. The electroproduction reactions performed in these experiments were studied at W and Q^2 regions of $1.3-2.8$ GeV and $0.3-1.4$ (GeV)^2, respectively, using the streamer chamber at DESY. Results obtained for inclusive electroproduction of positive and negative hadrons in the quark–fragmentation region supports the validity of the quark–parton model at surprisingly low Q^2 and W. After subtracting the contribution of the dominantly diffractive produced ρ^0–mesons from the inclusive spectra of $\pi^\pm$–mesons, these spectra can be related to the inclusive distributions of $\pi^\pm$–mesons from e^+e^- annihilation by [14]:

$$\frac{1}{\sigma_{(\gamma^V p)}}\frac{d\sigma}{dz}(\gamma^V p \to \pi^\pm X) \simeq \frac{1}{2}\frac{1}{\sigma_{(e^+e^-)}}\frac{d\sigma}{dz}(e^+e^- \to \pi^\pm X) \qquad (30)$$

The factor $1/2$ in Eq. (30) arises from the fact that two quarks are fragmenting in e^+e^- annihilation. The similar results for charged pion electroproduction was obtained in Refs. [13, 15] and for the neutral π^0–meson inclusive electroproduction in Ref. [12]. For the kinematic region of our proposal [*i.e.*, $1.2 < Q^2$ (GeV/c)$^2 < 2.5$ and $1.9 < W$ (GeV) < 2.5], the quark–parton representation is working well.

One of the most important and unsolved problems of modern strong interaction physics (non perturbative QCD) are the investigations of real and virtual photons interacting with matter (*e.g.*, quarks and gluons). The measurements of different mesons ($\pi^\pm$, $K^\pm$) from inclusive electroproduction spectra on nucleons (p,n) in the deep–inelastic region for relatively small values of Q^2 will allow us to obtain certain information about the interaction mechanisms of photons with quarks and gluons; as well as quark and antiquark soft–annihilation cross sections.

The analysis of experimental data available for $\pi^\pm$ and π^0 electroproduction on the proton shows that, beginning already in the deep–inelastic region (*i.e.* from $W > 2$ GeV), the functions for u and d quark fragmentating into $\pi^{\pm,0}$ mesons are independent of the value of W [28], and possibly, are in weak dependence with Q^2. Consequently, the inclusive spectra of $\pi^\pm$ and π^0 mesons obtained from nucleons, can be used to investigate the dependence of $D^{\pm,0}_{u,d}(z,Q^2)$ for both W and Q^2. In turn, we can then check the applicability of Altarelli-Parisi evolution equations at $Q^2 < (1-2)$ (GeV/c)^2 and investigate the transition from the perturbative QCD region into the non perturbative region (*i.e.*, the effects due to power corrections over Q^2, higher twists, *etc.*).

2.2 Pion Electroproduction from Nuclei

2.2.1 Theoretical Models: Color Transparency

A recent hypothesis by Brodsky and Mueller [32] point out some qualitative properties of A–dependent effects in which QCD color transparency plays an important role. According to their hypothesis, the virtual photon interacts with the component of the hadron wave function that is

characterized by a spatial size on the order of $r(Q^2) \le r_h$ where r_h is the radius of a conventional hadron. The spatial size of the hadron $r(Q^2) = r_h$, if $Q^2 \le N^2 m_c^2$, where N is the number of additive quarks and antiquarks in the hadron, m_c is some characteristic hadronic mass which, apparently determines the radius of quark color and gluon confinement $R_c \simeq 1/m_c$.

The virtual photon interacting with a hadron in the latter's rest system is characterized by the time interval $\tau_P \simeq \nu/Q^2$, after which the hadronic wave function component with transverse size of $r(Q^2) \sim \sqrt{N^2 m_c^2/Q^2} r_h$, or the color (quark-antiquark) dipole, receives the entire energy ν from the virtual photon. During the time interval $\tau_F \simeq \nu/N^2 m_c^2 \simeq (Q^2/N^2 m_c^2)\,\tau_P$ the system will turn into a normal-sized hadron with radius r_h [32, 33, 34, 35].

Let us consider the process $ep \to e'\pi^+ n$ on the nuclear protons. If the nuclear proton is considered as a free proton, then the reaction $ep \to e'\pi^+ n$ on the nuclear protons will allow us to determine the change in the pion–virtual photon interaction cross section while traversing the nucleus and possibly interacting with other nucleons in the nucleus. By measuring nuclear matter transparency with respect to the pion yield from the process $ep \to e'\pi^+ n$, we can obtain information about the change in the interaction cross section of pions with the nucleons in the nucleus and, hence, extract information about the the change in its transverse size. If there is no change in the interaction cross section, the value of nuclear matter transparency is expected to be close to the prediction of Glauber [36]; however, if the average size of the pion, and hence, the interaction cross section with internuclear nucleons decreases, then the nuclear transparency must be higher than the value determined from the Glauber model — this difference becomes larger as Q^2 increases.

The transparency of nuclear matter or the "color transparency" is given by

$$T_{\pi^+ n}(A,Q^2) = \frac{1}{Z}\frac{\sigma[eA \to e'\pi^+ n(A-1)]}{\sigma(ep \to e'\pi^+ n)}\,, \qquad (31)$$

and is defined as the ratio of the pion electroproduction cross section from the reaction $ep \to e'\pi^+ n$ with nuclear protons normalized to the proton number of the nucleus, to the cross section from the reaction $ep \to e'\pi^+ n$. Eq. (31) characterizes the propagation of pions through a nucleus. It is commonly assumed, that the motion of pions through a nucleus can be described by the Glauber approach [36]. Minimal transparency occurs in the case when the pion, passing through the nucleus, may interact with nucleons in nucleus with $\sigma_{\pi N}$ cross section, which coincides with the pion–nucleon interaction. If the "small-sized pion" interacts with the nucleons in the nucleus, the cross section σ is smaller than $\sigma_{\pi N}$ cross section of pion–nucleon interaction, $\sigma \le \sigma_{\pi N}$. The result is nuclear matter transparency being higher than the minimal value determined by the Glauber model. The maximum value of transparency equals unity at small values of $\sigma \simeq 0$, which may occur when $Q^2 \gg N^2 m_c^2$.

Nuclear matter transparency is defined by Refs. [36]:

$$T = \frac{1}{A}\int \rho(b,x)\exp\left[-\int_x^{+\infty}\rho(b,t)\sigma(t-x)dt\right]d\vec{b}\,dx, \qquad (32)$$

where

$$\rho(b,x) = \rho(r) = \frac{\rho_0}{1+\exp[(r-r_A)/a]}\,. \qquad (33)$$

Here, the Wood–Saxon nuclear matter density distribution normalized is to the condition $\int \rho(r) d^3\vec{r} = A$, the impact parameter $b = |\vec{b}|$, $r = \sqrt{b^2 + x^2}$, $a = 0.54$, and $r_A = (0.978 + 0.0206A^{1/3})A^{1/3}$ [34]. In Eq. (32), $\sigma(t)$ is the "small–size pion" interaction cross section with internuclear nucleons as a function of the space–time variable t. This value increases from σ_0 at the point $t = 0$ (this point is actually not a point, but is a space–time region with $\tau_P \simeq \nu/Q^2$ dimensions), where an electron–pion interaction or a virtual–photon was absorbed by a pion has taken place, to $\sigma_{\pi N}$ at $t \gg \tau_F$, where τ_F is the characteristic time of the color dipole (compressed or small–sized pion) in transition to a normal pion. In the framework of the color dipole hypothesis, $\sigma(t)$ is expected to be [32, 33, 35]:

$$\sigma(t) = \sigma_{\pi N}^{tot} - (\sigma_{\pi N}^{tot} - \sigma_0)\exp(-t^2/\tau_F^2) \tag{34}$$

where $\sigma_0 = (N^2 m_c^2/Q^2)\sigma_{\pi N}^{tot}$ and $\tau_F = \nu/N^2 m_c^2$. Here $\sigma_{\pi N}^{tot} = 30$ mb, which corresponds to the characteristic total cross section of the pion–nucleus interaction in the energy range of interest $\sim (1.5 - 4.0)$ GeV.

2.2.2 Theoretical Models: Quark Hadronization Mechanism

Investigation into mechanisms for quark and gluon hadronization (*i.e.*, the transition of color constituent quarks into colorless hadron states) is one of the central problems in modern elementary particle physics. The process of deep–inelastic leptoproduction in nuclei, contains interesting information about the process of hadron formation from constituents (quarks and gluons) as well as on the propagation of quarks and quark–gluon systems in nuclear matter [37, 38, 39, 34, 32, 33, 35].

At present, there is not a clear understanding of the mechanism for hadron formation from quarks and gluons, nor of the propagation for quarks in nuclear matter. The main difficulty here is the presence of strong interactions (non–perturbative QCD effects) in the final stages of hadron formation from quarks and gluons; however, in the presence of a hard subprocess with $Q^2 \gg m_c^2$ where m_c is some characteristic mass $m_c^2 \simeq 0.1$ GeV^2 [33, 35], the time that characterizes the virtual–photon quark hard subprocess

$$\tau_P \simeq \frac{\nu}{Q^2} \ , \tag{35}$$

is less than the time of transformation of the quark (quark–gluon system) produced in this subprocess to form into a normal–sized hadron at a characteristic time $\tau_F \simeq \nu/m_c^2$.

According to modern understanding, the virtual photon (ν, Q^2) interacts with the nucleonic quark during a time interval

$$\tau_P \simeq \frac{\nu}{Q^2} \sim \frac{1}{x_B} \ , \tag{36}$$

where $x_B = Q^2/2m_p\nu$ and m_p the nucleon mass. The interaction cross section $\sigma(t)$ of such a point–like quark (quark–gluon system [37, 38], or quark–antiquark color dipole [32]) evolves from [34, 32, 33, 35]:

$$\sigma_q = \left(\frac{N^2 m_c^2}{Q^2}\right)\sigma_h \ , \tag{37}$$

where N is the number of additive quarks and antiquarks in the final hadron, at a time $\sim \tau_P$ up to the hadron–nucleon interaction cross section σ_h at the instant of fast hadron formation (or recombination time) τ_F.

Different conceptions exist concerning the evolution of the color and composition of a quark–gluon system or parton jet that produces a fast or knocked–out quark in the electroproduction process. In Refs.[40, 41], a mechanism is offered, which makes the quark–gluon jet colorless in the interaction time interval $\sim \tau_P$. In the framework of such a picture, the quark–gluon system looks like a white quark–antiquark string having a fast quark and slow antiquark on its ends. Such a string starts its hadronization in time intervals on the order of τ_P, where the slow antiquark hadronizes and the wave of hadronization reaches the fast quark at the moment $\sim \tau_F$, when a leading hadron containing a fast quark is formed [40, 41].

Another scenario of fast–hadron formation is developed [32] whereby the leading hadron, which contains a fast quark, is formed during a time interval $\sim \tau_P$, but its transverse dimensions are $N^2 m_c^2/Q^2$ times smaller than the hadron size. Such a compressed color dipole transforms into a normal hadron in a time interval $\sim \tau_F$ and only then will its interaction cross section with the nucleons in the nucleus become equal to the hadronic cross section σ_h.

The general point in fast–hadron formation is the fact that during a time interval $\sim \tau_P$, a quark–gluon system (quark, quark–antiquark string, or colour dipole) is formed in a time τ_F that contains a leading (valence) quark of this system. The interaction cross section of such a system starts increasing from the value $\sigma_q \simeq (N^2 m_c^2/Q^2)\sigma_h$ at the moment τ_P up to the value σ_h at the moment τ_F of the leading hadron formation.

It is impossible to predict the behavior of $\sigma(t)$ from σ_q to σ_h in the framework of perturbative QCD — at least in the vicinity of $t \sim \tau_F$. At $Q^2 \gg m_c^2$ for $t \sim \tau_P$, one can make predictions for $\sigma(t) \sim t$[37, 34] in the framework of perturbative QCD; in the so–called model of quantum diffusion, the transverse dimension of quark–gluon system increases as $\sqrt{t}$, because in the transverse plane the production points of quark–antiquark pairs or gluons are on the trajectory of a Brownian particle. In the framework of another mechanism of hadronization, based on the concept of $q\bar{q}$ colored dipole formation at time $\sim \tau_P$, it is expected that $\sigma(t) \sim t^2$ [32]. There is a relatively small difference $\sim (5 - 10\%)$ [35] between the predicted transparency in these two models but, both give a significant deviation from the Glauber–type mechanism [36], which assumes that normal size hadrons are formed at the interaction point during a time interval τ_P. *The search for such a large deviation between a Q^2–dependent hadronization mechanism and the Glauber model is one of the main goals of this project.*

To probe the time scale for quark hadronization, we will measure the nuclear transparency T as a function of Q^2. The nuclear transparency T is defined as

$$T_h^d(A, Q^2, z) = \frac{2}{A}\frac{d\sigma(eA \to e'hX)\,/\,dz}{d\sigma(ed \to e'hX)\,/\,dz} \ , \tag{38}$$

where A is the nucleon number and D is the deuteron. Nuclear transparency reaches a minimum when the hadron is produced directly at the interaction point of an incident particle with the nucleus. In this case, the produced hadron h interacts with the usual $h - N$ cross section. The hadron propagation in the nucleus can then be described in the conventional Glauber model [36]. The transparency is equal to the probability for the hadron to exit the nucleus without interacting elastically.

To distinguish between rescattered and non-rescattered hadrons, it is necessary to restrict our attention to the high energy part of the inclusive spectrum (*i.e.*, to large values of the variable $z = E_h/\nu$, where E_h is the energy of the detected hadron). At relatively high values of the variable $z \geq (0.5 - 0.7)$, the dominant contribution to the inclusive hadron spectra is the direct production of hadrons. As shown in Refs.[17, 42] in the fragmentation region of different quark-gluon systems, the contributions from decays of mesonic resonances in the inclusive spectrum of π-mesons are less than (10–20)% in the range $z \geq (0.5 - 0.7)$; for this reason, the region of relatively high value of z is preferable, where the information on the mechanism of the photon-nucleon interaction as well as the propagation of quarks and/or hadrons through nuclear matter is carried by the direct hadrons.

If the hadronization process requires a finite space-time interval, then the transparency T will be higher than the minimal Glauber value [36]. The maximum value of T, is achieved when the hadron is formed outside the nucleus. If the mean absorption path of the virtual photon in nuclear matter exceeds the size of the nucleus (for values of $x_B > 0.05$ [43]), then the probability that the quark produced at time $\sim \tau_P$ and the fast hadron produced at time τ_F will not undergo inelastic interactions in the nucleus is determined by the expression Eq. (32). In the general case we need to take into account as inelastic as well as elastic interactions of the fast hadron in the nuclear matter. We will discuss the pions rescattering problem in the next subsection.

Here it is important to note that our picture of fast hadron formation assumes that $\sigma(\gamma^V A) \simeq A\sigma(\gamma^V N)$. Effects connected with the screening of the interaction of photons with nuclear matter should be absent. The experimental data on deep inelastic interactions of leptons with nuclei show that the relation $\sigma(\gamma^V A) \simeq A\sigma(\gamma^V N)$ is valid [44, 45, 46] over a wide range ($0.05 \leq x_B \leq 0.3$) of the Bjorken variable $x_B = Q^2/2m_p\nu$. Our investigations are within this range of x_B.

2.2.3 Theoretical Models: Rescattering of Pions

Rescattering of pions in the nucleus can be envisioned using the framework developed within the intra-nuclear cascade model (INC) [47, 48, 49, 50, 51, 52] or in the model by Glauber. To perform a calculation in the INC model, one needs to input the multiplicity of produced particles from the reactions $\gamma^V + N \to X$, the spatial coordinates of all particles, and their momenta. Cascades of produced particles can be simulated in the usual way. Also, one can take into account elastic and inelastic interactions, Fermi motions of the nucleons, the absorption of mesons by correlated (n, p) pairs, mesonic charge exchange, and so on. The end result is to obtain an exclusive description of the interactions.

Unfortunately, cascade codes are, as a rule, very large and written in old formalisms; however, some codes consider the production of mesonic and baryonic resonances in (πN)- and (NN)-interactions. The calculations of characteristic (γA)-interactions are not known. There are some attempts to simulate (νA)-reactions.

By in large, Glauber's model is much simpler for calculations of inclusive characteristics. The model describes extraordinarily well momentum spectra of protons in the reactions $p+A \to p+X$ at 19.2 and 24 GeV/c [53, 54, 55]. It also describes (πA) elastic scattering too. Although the calculation of momenta spectra of mesons is unknown, one hopes to obtain good results for $z \simeq x_F > 0.3$ because in this region the yield of leading particles dominates.

Following Refs. [53, 54, 55] it is easy to obtain the expression for the cross section of the

processes $\gamma^V + N \to \pi^\pm + X$ on intra-nuclear nucleons with n^{th} rescattering of $\pi^\pm$-mesons

$$\frac{d^3\sigma}{d\vec{p}}(\gamma^V A \to \pi^\pm X) = \int \frac{d^3\sigma(\gamma^V N \to \pi^\pm X)}{d\vec{p}_0}\delta(\vec{p} - \vec{p}_0 - \sum_{i=1}^{n}\vec{p}_i)\prod_{i=0}^{n}\omega(\vec{p}_i)d\vec{p}_i$$
$$\int d\vec{b}\int_{-\infty}^{+\infty}\rho_A(\vec{b}, x)\,dx\frac{\left[\sigma_{\pi N}^{tot}L(\vec{b}, x+\tau_F, \infty)\right]^n}{n!}\exp[-\sigma_{\pi N}^{tot}L(\vec{b}, x+\tau_F, \infty)] \ . \qquad (39)$$

Here ρ_A is the nuclear density as given in Eq. (33), $\sigma_{\pi N}^{tot}$ is the total cross section of the (πN)-interaction, and L is the thickness function of the nucleus given by

$$L(\vec{b}, x_1, x_2) = \theta(x_2 - x_1)\int_{x_1}^{x_2}\rho_A(\sqrt{b^2 + x^2})dx \ , \qquad (40)$$

where τ_F is the formation length, b is impact parameter, $\omega(\vec{p})$ is the momentum distribution of $\pi^\pm$-meson from the reaction $\pi^\pm + N \to \pi^\pm + X$.

The first integral in Eq. (39) describes the change in the π-meson spectra produced in a nucleon. The second integral is proportional to the probability of the n^{th} rescattering. It is obvious that this probability decreases with increasing formation length. Figure 6 displays the rescattering probabilities as a function of formation length.

Let us examine this phenomena on a purely qualitative level by considering what is happening in Figs. 16 and 21 in Section III of this proposal. The π^+ meson spectra from $(\gamma^V p)$-interactions has a bump in the region of $z \simeq 0.95$, a dip at $z \simeq 0.8 - 0.9$, and the cross section increases at $z < 0.8$. In the region $z \simeq 0.95$, elastic rescattering leads to a softness of the spectra and fills the dip at $z \simeq 0.8-0.9$. In the region of $z < 0.8$ there is a competition between two yields. The cross section in this region at any defined z has a positive yield from more energetic mesons produced in $(\gamma^V N)$ reactions which suffer inelastic interactions within the nucleus. On the other hand, the number of mesons is decreasing due to elastic and inelastic rescatterings. The dominance of the first or second yield depends on the value of z and on the formation length τ_F.

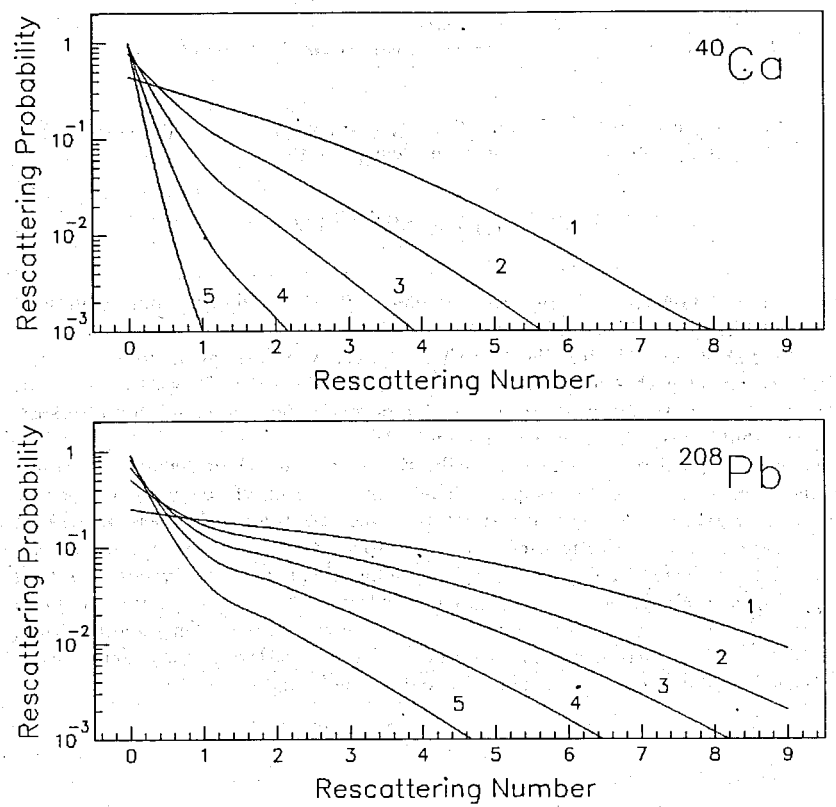

Fig. 6 Rescattering probability dependence on the number of rescatterings for different formation times (or lengths) τ_F. Curves 1 – $\tau_F = 0$ (Glauber), curves 2 – $\tau_F = 3$ fm, curves 3 – $\tau_F = 5$ fm, curves 4 – $\tau_F = 7$ fm and curves 5 – $\tau_F = 10$ fm.

2.2.4 Prior Experiments

There have been very few experiments studying the inclusive leptoproduction of hadrons in atomic nuclei. Reported in Ref.[56] for the first time was the increase of transparency (decrease of absorptive power) in the yield of fast charged products of the virtual photon hadronization from the nucleus; however, these data failed to provide sufficient detailed information on the parameters that characterize the space-time picture for the process of hadron formation. The primary causes for not pinning down the effect were due to low statistics and an averaging of the data over very wide intervals of ν and Q^2.

In another experiment conducted by EMC [57] at CERN using muon beams with $E_\mu = 200$ GeV, charged hadrons were detected in the virtual-photon fragmentation region. At $\nu \simeq 100$ GeV and higher, a nearly full transparency of nuclear matter to the leptoproduction of hadrons was observed. The analysis of these experiments as well as the antineutrino experiment at energies of $E_{\bar{\nu}} < 30$ GeV [58] does not permit one to obtain definite information about the characteristic time scales of the quark hadronization process. Thus, estimates of the parameter m_c^2 obtained in Refs.[57, 58] are (0.08 ± 0.04) and ~ 2.0 GeV^2, respectively. The data obtained in Ref.[57] at large values of z (~ 0.7) are of low statistical accuracy.

It follows from the analysis [35] of the SLAC and EMC CERN data that the dependence $\sigma_q = (N^2 m_c^2/Q^2)\sigma_h$ (where $N = 2$ is the number of valence quarks in the mesons) describes the experimental results at $m_c{}^2 = 0.11 \pm 0.01$ GeV^2. The time of quark hadronization τ_F does not depend upon the energy of the final meson and is determined only by the energy ν of the quark (i.e., $\tau_F = \nu/m_c^2$). Because of the precision of the experiments [$\sim (10-15)\%$], an estimate could be made about the parameter m_c^2 to an accuracy of about 10%. The level of accuracy achieved here can permit the possibility of distinguishing between different theoretical models.

Setup	E_e (GeV)	θ_e (deg)	θ_π (deg)	$P_\pi^{(a)}$ (GeV)	$P_\pi^{(b)}$ (GeV)	$P_\pi^{(c)}$ (GeV)	$P_\pi^{(d)}$ (GeV)
1	3.9	13.0	21.0	1.45	1.85		
2	3.0	18.0	16.0	2.00	2.35	2.75	
3	2.1	24.0	12.0	2.50	2.85	3.25	3.65

Table 2: The nine kinematic points at $E_{beam} = 6.0$ GeV and $x_B = 0.30$

3. The Experiment

3.1 The Goals and Kinematic Condition

Experimentally, we detect the electroproduced pion in coincidence with the scattered electron. In Hall A, the two HRS spectrometers will be utilized.

The main goals of the project are:

1. Measurements of $\pi^{\pm}$–meson electroproduction on ^{1}H, and π^+–meson electroproduction on ^{2}H, ^{40}Ca, and ^{208}Pb nuclei in the kinematic range $x_B \simeq 0.3$, $1.0 \leq Q^2(\mathrm{GeV}/c)^2 \leq 2.5$ and $0.6 \leq z \leq 1.0$.

2. Determine the contributions from Δ and ρ hadronic resonances to the inclusive spectra of pions and their dependence on Q^2.

3. Investigating the dependence of the electroproduced pion charge asymmetry $\eta(z, Q^2)$ from the proton data on Q^2 and z.

4. Search for a large deviation between a Q^2–dependent hadronization mechanism and the Glauber model.

5. Obtain the characteristic time for quark hadronization from our nuclear matter transparency analysis.

6. Examine the nuclear color transparency with respect to the π^+–mesons moving through nuclear matter.

7. Determine the quark–antiquark annihilation cross section from our $\eta(z, Q^2)$ analysis.

As stated earlier, we would like to perform the experiment at $x_B \simeq 0.3$. The choice for $x_B \simeq 0.3$ is related to the nucleon as well as to the nuclear programs of our proposal. First of all, the experimental data on the nucleon structure functions $F_2(x_B, Q^2)$ show that at $x_B \simeq 0.3$, the value of $F_2(x_B, Q^2)$ is practically independent of Q^2 for our kinematic region 1.0 GeV$^2 \leq Q^2 \leq 2.5$ GeV^2, see for example Ref.[59]. Because we would like to concentrate on the quark–fragmentation functions and on the Q^2 dependence of the charge asymmetry, it is important to have $F_2(x_B, Q^2) \sim$ *constant* for the kinematic region of our experiment.

Another reason is that the nucleus and nucleon structure function ratio $F_2^A(x_B)/F_2^D(x_B) \simeq 1$ at $x_B \simeq 0.3$, see for example Ref. [44]. The pion production cross section depends on the $(\gamma^V N)$–interaction cross section, as well as the quark to pion fragmentation functions. Because in the nuclear part of this project, we propose to study pion propagation in nuclear matter and would like to have the condition $\sigma^{tot}(\gamma^V A)/A \simeq \sigma^{tot}(\gamma^V D)/2$ or $F_2^A(x_B)/F_2^D(x_B) \simeq 1$ in the kinematic region of our proposal. So the condition $x_B \simeq 0.3$ will allow us to interpret the difference between nuclear transparency with respect to π^+–meson production from the unit as a result of the π^+–mesons and quarks propagating through nuclear matter.

To allow us to achieve our goals, we propose to make our coincidence electron–π–meson measurements at nine configurations using the Hall A HRS2 spectrometer system. Moreover, we need only to make two additional position changes for the last two spectrometer configurations; also with these position configurations, a set of magnetic field changes would be made to both spectrometers with more of the changes occurring on the hadron arm. The angular positions and particle momenta for the electron and hadron arms, respectively, are listed in Table 2. With the limitations imposed by the HRS2 system, the arrangements listed in Table 2 denote the minimum group of configurations that will allow us to make our coincidence measurements in the proposed range of z and Q^2. Figure 7 shows the region in the $(z \times Q^2)$ plane which can be covered with our proposed nine kinematic measurements. Thus we can obtain data in the range $1.0 \leq Q^2(\mathrm{GeV}/c)^2 \leq 2.5$ and $0.6 \leq z \simeq 1.0$.

In each small box with size $\Delta z = 0.05$ and $\Delta Q^2 = 0.1$ GeV^2 in Fig. 7, we propose to obtain $N_{ev} \simeq 10000$ events. The **1a** and **1b** setups in Table 2 cover (0.95 GeV$^2 \leq Q^2 \leq$ 1.55 GeV^2)$\times$(0.6 $\leq z \leq$ 0.8) and (0.95 GeV$^2 \leq Q^2 \leq$ 1.55 GeV^2)$\times$(0.8 $\leq z \leq$ 1.0), respectively. From each of these setups we propose to obtain $N_{ev} \simeq 240000$ events. Distributions for Q^2, x_B, W, and ε for setups **1a** and **1b** are shown in Fig. 8. Setups **2a**, **2b**, and **2c** cover (1.45 GeV$^2 \leq Q^2 \leq$ 2.05 GeV^2) $\times$ (0.6 $\leq z \leq$ 0.74), (1.45 GeV$^2 \leq Q^2 \leq$ 2.05 GeV^2) $\times$ (0.74 $\leq z \leq$ 0.87), and (1.45GeV$^2 \leq Q^2 \leq$ 2.05 GeV^2) $\times$ (0.87 $\leq z \leq$ 1.00), respectively, and from each of these setups, we plan to obtain $N_{ev} \simeq 160000$ events. The final setup **3a**, **3b**, **3c** and **3d** are cover in the $(z \times Q^2)$ plane (2.05 GeV$^2 \leq Q^2 \leq$ 2.55 GeV^2) $\times$ (0.6 $\leq z \leq$ 0.7), (2.05 GeV$^2 \leq Q^2 \leq$ 2.55 GeV^2) $\times$ (0.7 $\leq z \leq$ 0.8), (2.05 GeV$^2 \leq Q^2 \leq$ 2.55 GeV^2) $\times$ (0.8 $\leq z \leq$ 0.9), and (2.05 GeV$^2 \leq Q^2 \leq$ 2.55 GeV^2) $\times$ (0.9 $\leq z \leq$ 1.0), respectively. From the each of these setups we plan to obtain $N_{ev} \simeq 120000$ events. The total number of events then is $N_{ev}^{tot} \simeq 1440000$ events for each target and each type of pion. The beam time request is presented in Section 3.5.

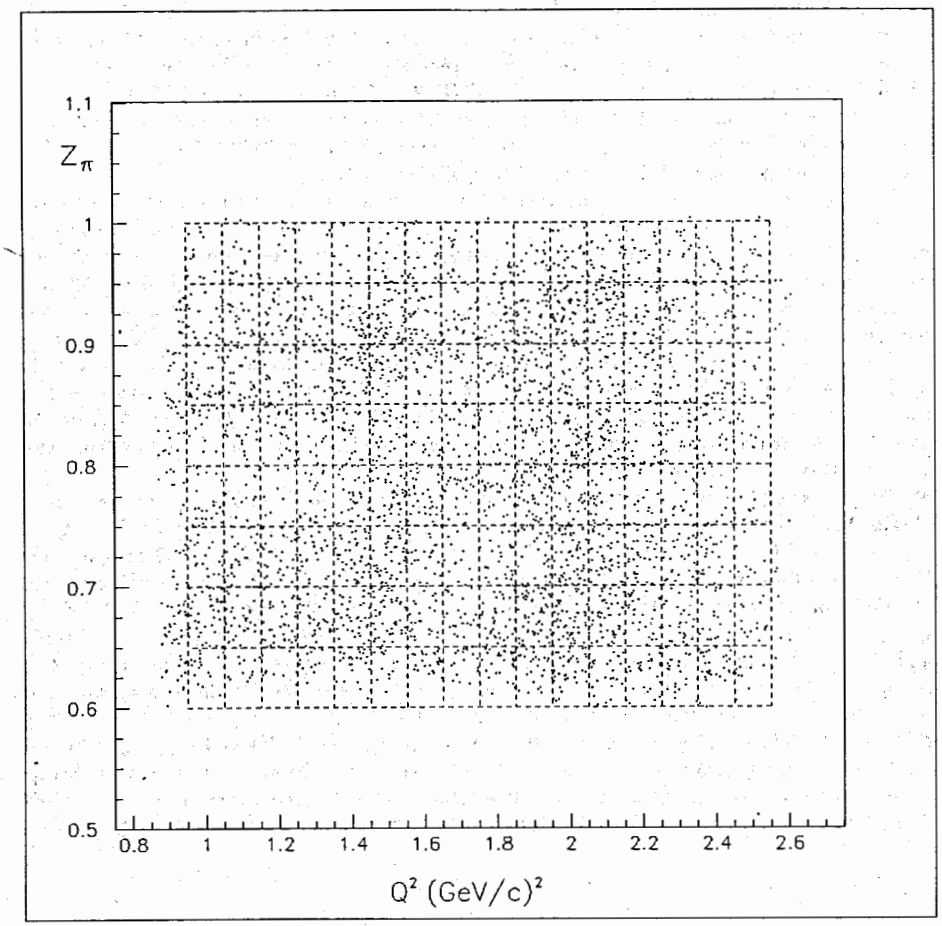

Fig. 7 Event distribution on a $(z \times Q^2)$ plot from the nine kinematic setups **1a**, **1b** at $Q^2 \simeq 1.2$ (GeV/c)^2, **2a**, **2b** and **2c** at $Q^2 \simeq 1.7$ (GeV/c)^2 and **3a**, **3b**, **3c** and **3d** at $Q^2 \simeq 2.2$ (GeV/c)^2. For each box with dimensions $\Delta z = 0.05$ and $\Delta Q^2 = 0.1$ (GeV/c)^2, we plan to have 10^4 events.

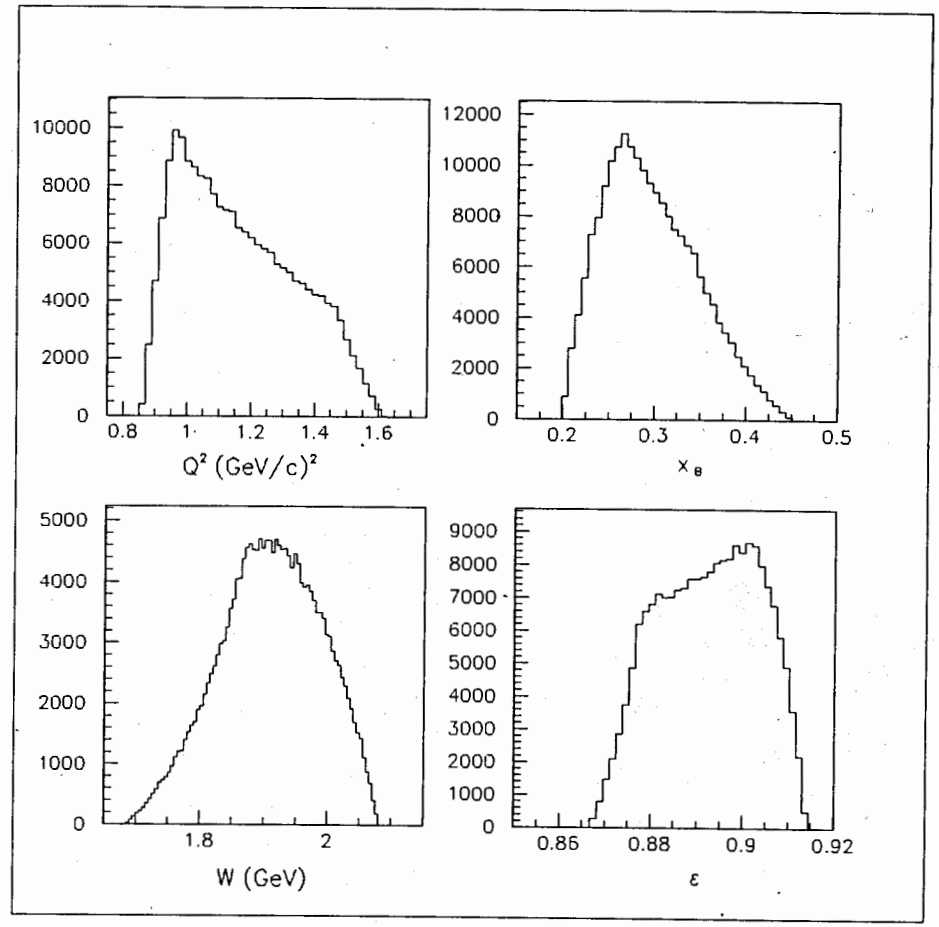

Fig. 8 Distributions for the kinematic variables Q^2, x_B, W and, ε for the **1a** and **1b** setups of this proposed experiment.

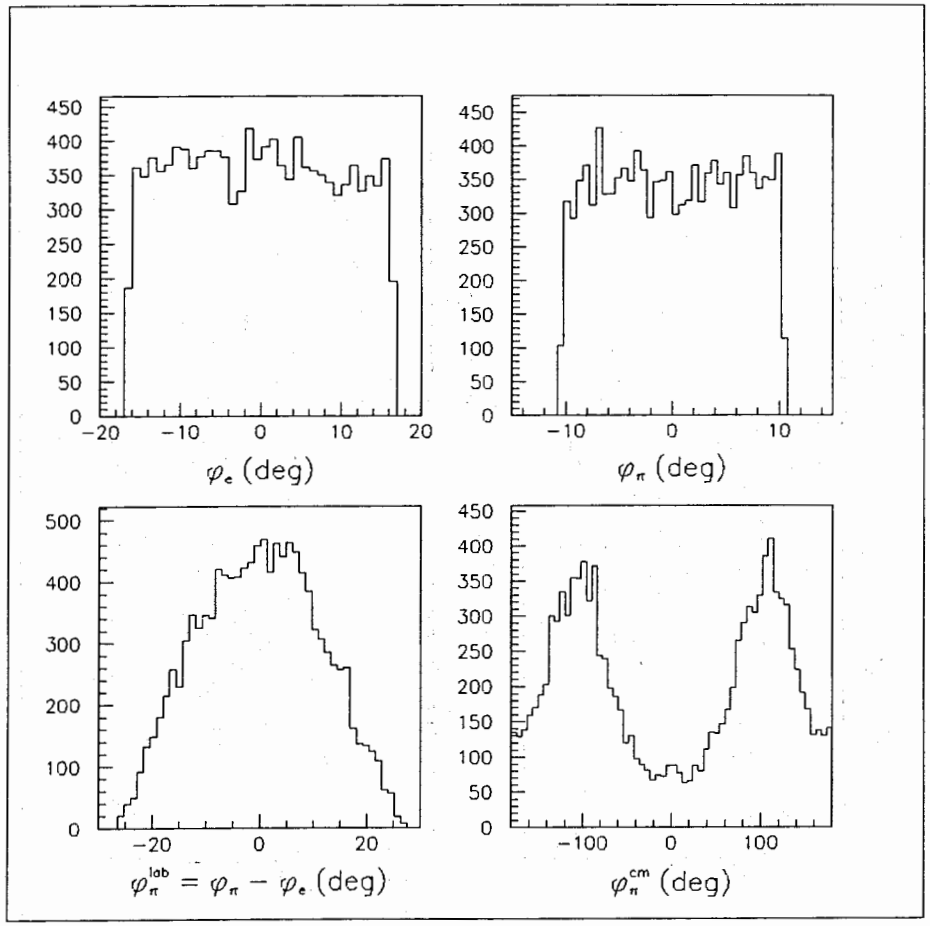

Fig. 9 Azimuthal angle distributions for the electron (ϕ_e) and hadron (ϕ_π) arms, respectively. Also shown are the distribution of angles in the laboratory system (ϕ_π^{lab}) between the π–meson production and the electron scattering planes, and with respect to the ($\gamma^V p$) center–of–mass system. The two peaks in the ϕ_π^{cm} spectrum, correspond to $-90°$ and $+90°$ (*i.e.*, pion production below and above the electron scattering plane).

3.2 The Experimental Procedure / Condition

We plan to investigate the inclusive $\pi^{\pm}$–electroproduction spectra at $x_B = 0.30$. The scattered electrons will be detected by one HRS spectrometer, while the charged mesons by the other HRS spectrometer [60]. The two spectrometer configuration allows us to perform measurements in the kinematic region of interest. The spectrometer detector stacks use standard focal plane instrumentation and are detailed in the CEBAF.CDR [60]. There will be drift chambers for charged particle tracking, a gas Čerenkov detector for particle identification, scintillator hodoscopes for fast timing, and Pb–glass shower counters for calorimetry and additional π/e discrimination. The momentum of the particle will be determined by reconstructing its trajectory through the dipole magnet while the production angles are then obtained by tracing the trajectory back to the interaction position in the target.

Special consideration for the hadron arm must be taken into account because of the large background from $(e, e'p)$ coincidence events. A suppression by a factor of $\sim 10^3$ is expected by utilizing an aerogel Čerenkov counter in the hadron arm. A prototype aerogel Čerenkov counter was tested at Saclay late in 1993. The index of refraction of $n = 1.025$ in the aerogel Čerenkov counter provides a threshold of 4.17 GeV/c for protons and 0.62 GeV/c for pions; therefore, for hadron momenta up to 4.0 GeV/c, the aerogel Čerenkov should provide an excellent tool for discriminating against protons. Also, because the number of photons produced in the Čerenkov process increases with momentum, the aerogel Čerenkov efficiency will increase and thereby provide greater reliability for discerning protons from π–meson events. Low discriminator thresholds for photomultiplier signals will also help insure the best possible particle identification for the lowest pion momenta.

Cryogenic hydrogen and deuterium, as well as solid calcium targets will be used. The ^{40}Ca target is very convenient for future analysis where we will use it for comparison with deuterium data because it consists of equal numbers of protons and neutrons. For absolute calibration, it is necessary for some experimental points to take measurements of elastic electron scattering on hydrogen. For backgrounds from the walls of the cryogenic target cell, it is necessary to take measurements with an empty target cell.

It is important to have both the liquid and the solid target data taken with the same magnetic field settings for the spectrometers. This restriction will suppress any systematic uncertainties that may arise from changing the fields during off–line analysis. Listed in Table 3 are the parameters for the HRS2 system for electron and hadron observation.

ELECTRON BEAM PARAMETERS

Incident energy	6.0 GeV
Beam energy spread	$\leq 0.1\%$
Duty–factor	100%
Incident electron intensity	(50–170)μA

The beam intensity is limited by the singles rate in the the hadron arm and the predicted accidental coincidence count rate level. Both quantities are well within acceptable tolerances of the HRS system, and experimentally, the estimated reals–to–accidental levels are quite reasonable for all Q^2 points.

Parameters	HRS (Electron)	HRS (Hadron)
Optical Length	22.8 m	22.8 m
Momentum Range	(0.2–0.3)–4.0 GeV/c	(0.2–0.5)–4.0 GeV/c
Momentum Acceptance	10%	10%
Momentum Resolution	1×10^{-4}	1×10^{-4}
Angular Range	$10° - 165°$	$10° - 130°$
Target Length Acceptance	$\sim \pm 5$ cm	$\sim \pm 5$ cm
Angular Resolution (Horizontal)	0.5 mr	0.5 mr
Angular Resolution (Vertical)	1.0 mr	1.0 mr
Horizontal Angular Acceptance	± 30 mr	± 30 mr
Vertical Angular Acceptance	± 65 mr	± 65 mr
Solid angle	7.8 msr	7.8 msr
Transverse Length Acceptance	± 5 cm	± 5 cm
Transverse Position Resolution	0.1 cm	0.1 cm

Table 3: Parameters for the two Hall A HRS spectrometers. Note: the HRS spectrometers have parallel–to–point focussing in the scattering plane. The quoted values for the position resolutions include effects from finite beam size and detector resolutions.

3.3 Physics Backgrounds

To measure pion electroproduction from nuclei at CEBAF energies, it is important to know the contributions to the inclusive spectra of pions from hadronic–resonance decays as well as from processes of pions rescattering inside the nucleus. In these upcoming subsections, we consider possibilities to distinguish between pions that are electroproduced directly from the virtual photon–quark interaction from those pions that are produced from different hadronic–resonance decays as well as from those pions that multiply scatter in the nuclear medium.

3.3.1 Resonances Contributions

Consider the Δ and ρ resonance contributions to the channel $ep \to e'\pi^+\pi^- p$. We can separate these processes in an $(e, e'\pi^-)$ coincidence measurement by employing a missing mass off–line cut $M_x < (m_p + m_\pi)$. In Refs.[10, 11], a maximum likelihood fit to the experimental data by the Dalitz–density plot method was performed to obtain fit parameters which signify the strength of the different resonance and phase space (PS) contributions to the inclusive spectra of pions: they obtained, $a_{\Delta^{++}} = (25 \pm 3)\%$, $a_{\Delta^0} = (4 \pm 2)\%$, $a_\rho = (30 \pm 10)\%$ and $a_{PS} = (41 \pm 6)\%$ for the Δ^{++}, Δ^0, ρ channels, and (PS) contributions, respectively. These values were obtained for $0.8 < Q^2$ (GeV/c)$^2 < 1.4$ and $1.7 < W$ (GeV) < 2.0. Clearly, these parameters obtained in the above kinematic range cover our proposed points **1a** and **1b** of our experiment which have $Q^2 \simeq 1.2$ (GeV/c)^2 and $W \simeq 1.9$ GeV. It is important to note that the above values for $a_{\Delta^{++}}$, a_{Δ^0}, a_ρ and a_{PS} yield Δ, ρ, and phase–space contributions for a 4π acceptance for the final–state hadrons (see Fig. 2). These values of course change for different angular and momenta intervals. To acquire the proper Δs, ρ, and phase–space contributions for our hadron arm, we simulated the process $ep \to e'\pi^+\pi^- p$ using our proposed experimental configuration. The results of this simulation for the angular acceptance $\Delta\Omega_\pi$ ($\vartheta_{\pi^-} = 13.0°$) and for the **1a** setup are shown in Figs. 10 and 11 and Figs. 12 and 13, respectively.

Fig. 14 shows the contributions from the $\gamma^V p \to \pi^- \Delta^{++}$, $\gamma^V p \to \pi^+ \Delta^0$, $\gamma^V p \to \rho^0 p$ channels, and from phase space (PS) to the π^-–mesons spectra for full phase space acceptance (4π) for hadrons (a) and in our hadron arm (b) at $Q^2 \simeq 1.2$ (GeV/c)^2. The results show that for the kinematic region of interest $0.6 \leq z_\pi \leq 1.0$, contributions from Δ^{++} and ρ^0 resonances are important. Resonance contributions to the spectra of π^-–mesons decreases as Q^2 increases (see Fig. 15). For the high Q^2 point of our proposal [$Q^2 \simeq 2.5$ (GeV/c)^2], the Δ^{++} and ρ^0 contributions to the π^-–mesons spectra are 12% and 9%, respectively, for the acceptance given for setup **1a**. To obtain the results shown in Fig. 15, we use the experimental parametrization for Δ [11] and ρ^0 [10] in the framework of the vector dominance model (VDM):

$$\sigma_\Delta(Q^2) \sim \frac{1}{(1 + Q^2/m_\rho^2)^2} \tag{41}$$

$$\sigma_\rho(Q^2, W) \sim \frac{W^2 - m_p^2}{\sqrt{(W^2 - m_p^2 - Q^2)^2 + 4W^2Q^2}} \frac{1 + \varepsilon\xi^2 Q^2/m_\rho^2}{(1 + Q^2/m_\rho^2)^2} , \tag{42}$$

with $\xi^2 = 0.4$ [10] and the ρ–meson mass m_ρ.

Now let us consider resonance contributions to the inclusive π^+–meson spectra. Employing an off–line missing mass cut $M_x < (m_p + m_\pi)$ we can separate out the following processes

Acceptance	$a_{\Delta^{++}}$	a_{Δ^0}	a_ρ	a_{PS}
	%	%	%	%
4π	25.0	3.4	27.7	43.9
$\Delta\Omega_\pi$	24.4	3.7	27.9	44.0
$\Delta\Omega_\pi \Delta P_\pi$	39.2	0.4	22.9	37.5

Table 4: Resonance Parameters

$\gamma^V p \to \pi^+ n$, $\gamma^V p \to \pi^+\pi^- p$ and, $\gamma^V p \to \pi^+\pi^0 n$. The $\gamma^V p \to \pi^+ n$ channel can be studied in the framework of the Born approximation. The process $\gamma^V p \to \pi^+\pi^- p$ has been discussed above and results have already been shown. The process $\gamma^V p \to \pi^+\pi^0 n$ related to $\gamma^V p \to \pi^+\pi^- p$ by isotopic relations. For the deuterium case, we have

$$\begin{aligned}\sigma(\gamma^V d \to \pi^+ X) &\simeq \sigma(\gamma^V p \to \pi^+ X) + \sigma(\gamma^V n \to \pi^+ X) \\ &\simeq \sigma(\gamma^V p \to \pi^+ X) + \sigma(\gamma^V p \to \pi^- X) \ . \end{aligned} \tag{43}$$

The resulting π^+–mesons distributions from proton and deuterium are presented in Figs. 3 and 16 (b).

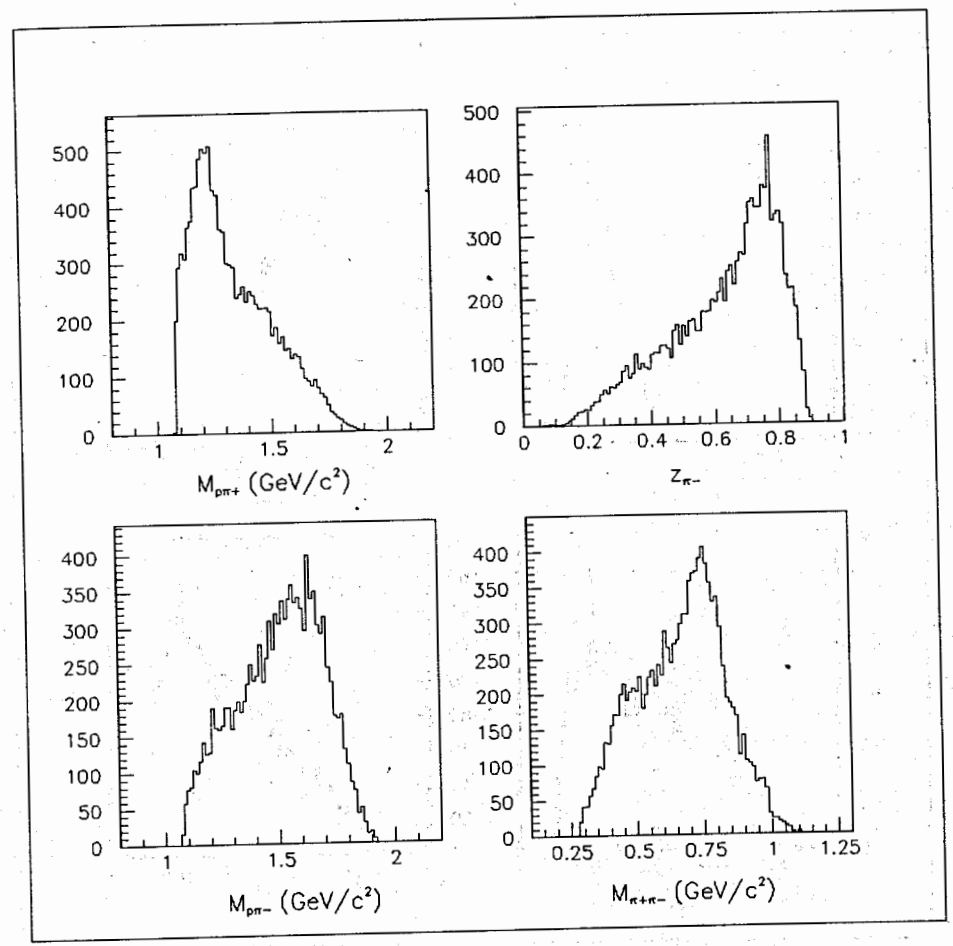

Fig. 10 Effective mass distributions for the $M_{p\pi^+}$ system, $M_{p\pi^-}$ system, $M_{\pi^+\pi^-}$ system, and distribution for z_{π^-} from the reaction $\gamma^V p \to \pi^-(\pi^+ p)$ for a hadron arm angular acceptance $\Delta\Omega_\pi$ ($\vartheta_{\pi^-} = 13.0°$). The values for the parameters $a_{\Delta^{++}}$, a_{Δ^0}, a_ρ, and a_{PS} are given in Table 4.

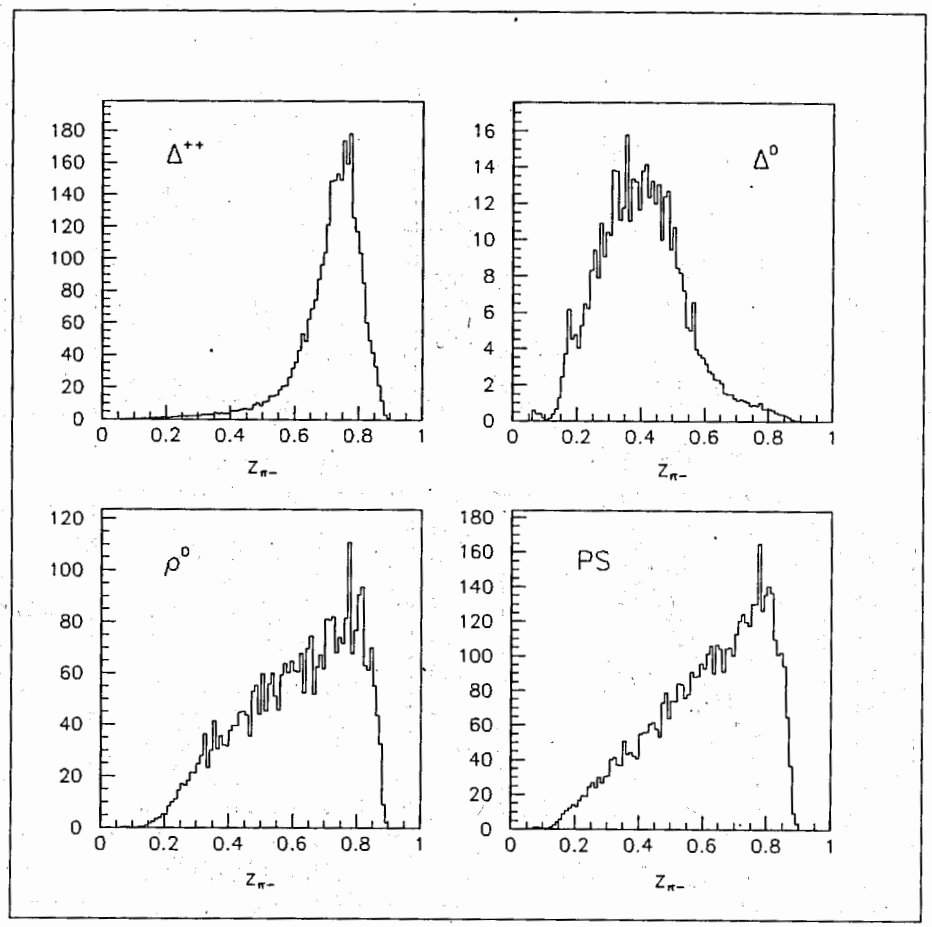

Fig. 11 z_{π^-} distributions in the hadron arm ($\vartheta_{\pi^-} = 13.0°$) from the $\gamma^V p \to \pi^- \Delta^{++}$, $\gamma^V p \to \pi^+ \Delta^0$, $\gamma^V p \to \rho^0 p$ channels, and from the $\gamma^V p \to \pi^+ \pi^- p$ reaction with a uniform event distribution on a Dalitz plot.

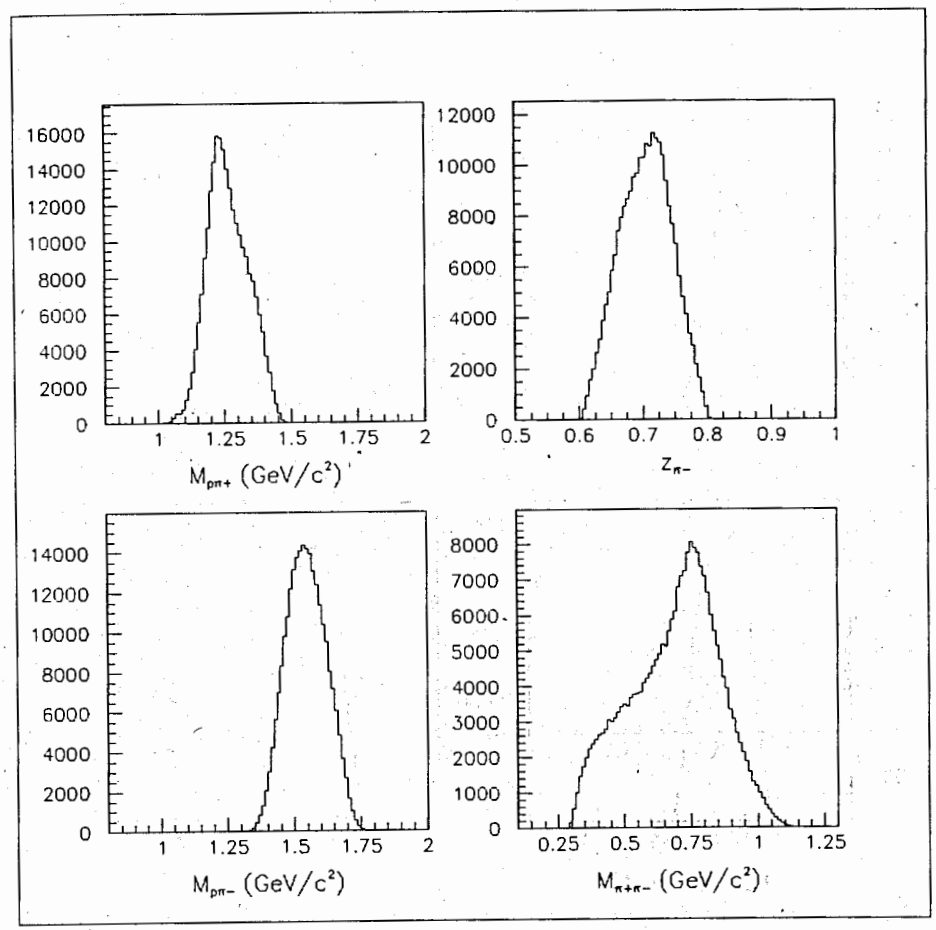

Fig. 12 Effective mass distributions $M_{p\pi^+}$, $M_{p\pi^-}$, $M_{\pi^+\pi^-}$, and a z_{π^-} distribution from the $\gamma^V p \to \pi^-(\pi^+ p)$ reaction in the acceptance $\Delta\Omega_\pi \times \Delta P_\pi$ ($\vartheta_{\pi^-} = 13.0°$ and $P_\pi = 1.45$ GeV/c). These spectra are predictions for the **1a** setup.

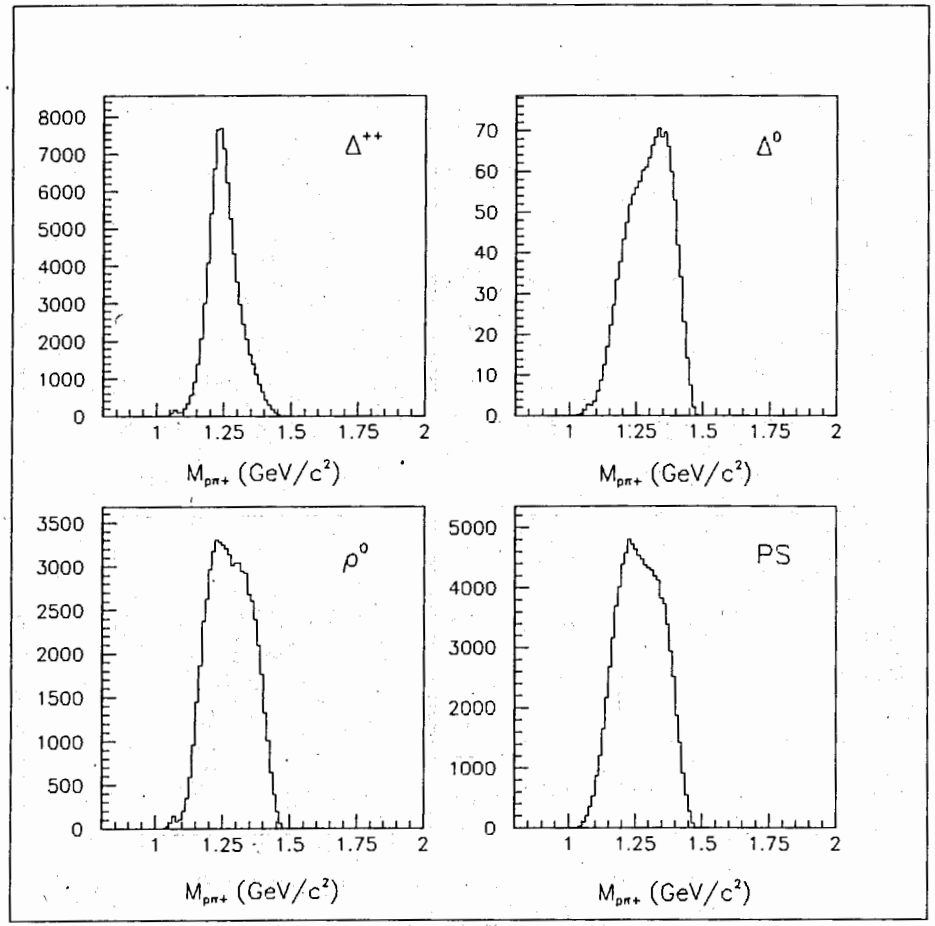

Fig. 13 $M_{p\pi^+}$ or M_x distributions for the channels $\gamma^V p \to \pi^- \Delta^{++}$, $\gamma^V p \to \pi^+ \Delta^0$, $\gamma^V p \to \rho^0 p$, and for the $\gamma^V p \to \pi^+ \pi^- p$ reaction with a uniform event distribution on a Dalitz plot. Distributions are for the kinematic setup **1a**.

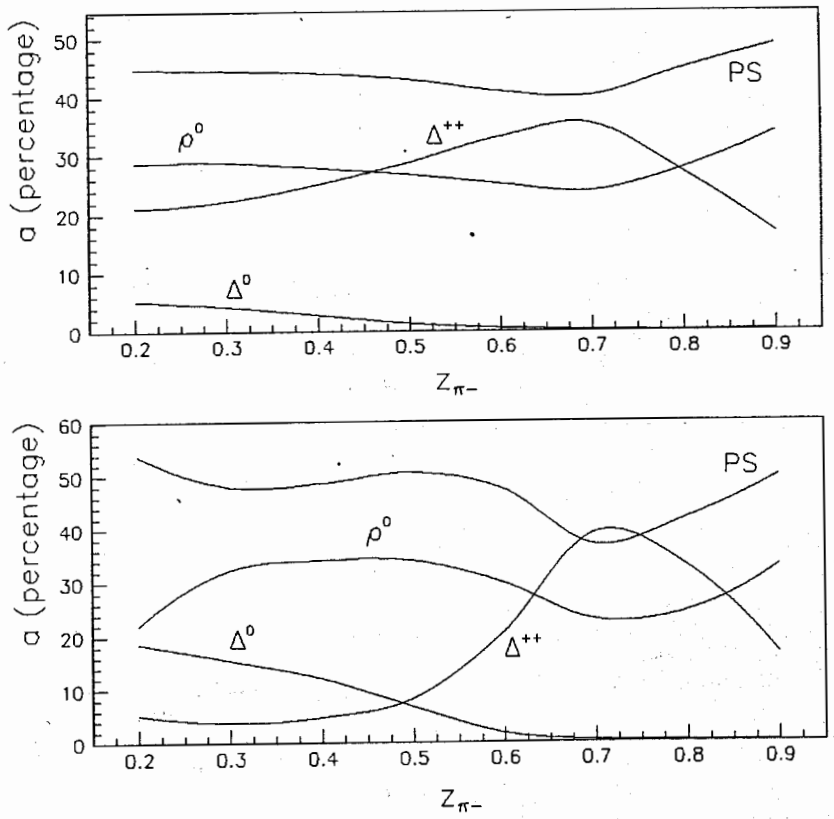

Fig. 14 Percent contributions from the channels $\gamma^V p \to \pi^- \Delta^{++}$, $\gamma^V p \to \pi^+ \Delta^0$, $\gamma^V p \to \rho^0 p$, and phase space (PS) contributions to the $\gamma^V p \to \pi^+ \pi^- p$ total cross section at a 4π hadronic acceptance (top) and for an angular acceptance $\Delta\Omega_\pi$ (bottom). The distributions are for $Q^2 \simeq 1.2$ (GeV/c)^2 and $\vartheta_{\pi^-} = 13.0°$ (our **1a** and **1b** setups).

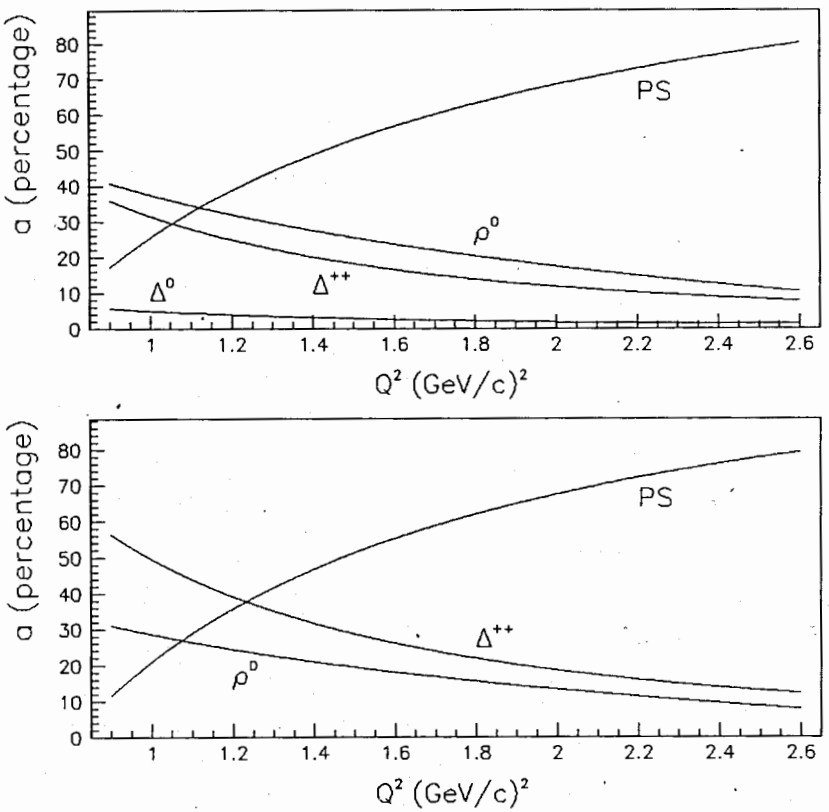

Fig. 15 Percent contributions from the channels $\gamma^V p \to \pi^- \Delta^{++}$, $\gamma^V p \to \pi^+ \Delta^0$, $\gamma^V p \to \rho^0 p$, and phase space (PS) contributions as a function of Q^2 to the $\gamma^V p \to \pi^+ \pi^- p$ total cross section for an angular acceptance $\Delta\Omega_\pi$ (top) and for an angular and momentum acceptance $\Delta\Omega_\pi \times \Delta P_\pi$ (bottom) for the **1a** setup in our proposed experiment.

3.3.2 Multiple Scattering

To estimate the rescattering of pions, we calculated the cross sections according to Eq. (39). The nuclear density $\rho(r)$ was taken to be the form given by Eq. (33). The rescattering calculations neglect the energy dependence of the total (πN)-interaction cross section; instead we used $\sigma_{\pi N}^{tot} = 30.0$ mb for the energy region of interest; namely, $\sim (1.5-4.0)$ GeV [59]. The distribution

$$\omega(\vec{p}) = \frac{1}{\sigma_{\pi N}^{tot}} \left(\frac{d^3\sigma^{el}}{d\vec{p}} + \frac{d^3\sigma^{in}}{d\vec{p}} \right) , \tag{44}$$

was calculated from a Monte Carlo simulation. The momentum distributions for the elastically scattered mesons was determined by the invariant squared four-momentum transfer t, and in the case of meson inelastic scattering, the distribution is determined by the Feynman variable $x_F \simeq 2p_z/\sqrt{s}$ and the meson transverse momentum p_T . In our simulation for elastic and inelastic scattering electroproduced π-mesons, the chosen distributions were [61, 10]:

$$\frac{d\sigma^{el}}{dt} \simeq \exp(At) \tag{45}$$

and

$$\frac{d\sigma^{in}}{dx_F\, dp_T^2} \simeq (1 - x_F)^3 \exp(-Bp_T^2) , \tag{46}$$

respectively, where $A = 6$ (GeV/c)$^{-2}$ and $B = 4$ (GeV/c)$^{-2}$.

For the energy region of our experiment, the main contribution to the inelastically produced π-mesons from the reaction $\pi N \to \pi X$ come from soft interactions at small p_T. The experimental data on the inclusive spectra of π-mesons with small p_T, are well described by Eq. (46) [61]. In other words, after the pion scatters inelastically, its momentum decreases and the direction of flight changes only slightly. On the other hand, if the pion scatters elastically (*i.e.*, $\pi N \to \pi N$) its direction of the flight may greatly change, but its momentum stays approximately the same Eq. (45). As we have already discussed in Section II.2.3, the inclusive spectra of π-mesons will change after multiple-scattering processes have ocurred in nuclei — the high momentum region of the spectra has decreased; whereas the low momentum region of the spectra has increased. We can see these changes in Fig. 16 and Fig. 21 for the reaction $\gamma^V A \to \pi^\pm X$. In the kinematic range of our experiment, $0.6 \leq z \leq 1.0$, the pion yields are decreasing, but the decrease is as small as the formation time τ_F is high.

Changes in the pion flight direction are illustrated in Fig. 17. From Fig. 17, we observe that the flight direction of the produced pion after multiple scattering in the nuclear medium will still be directed towards the acceptance of the hadron arm.

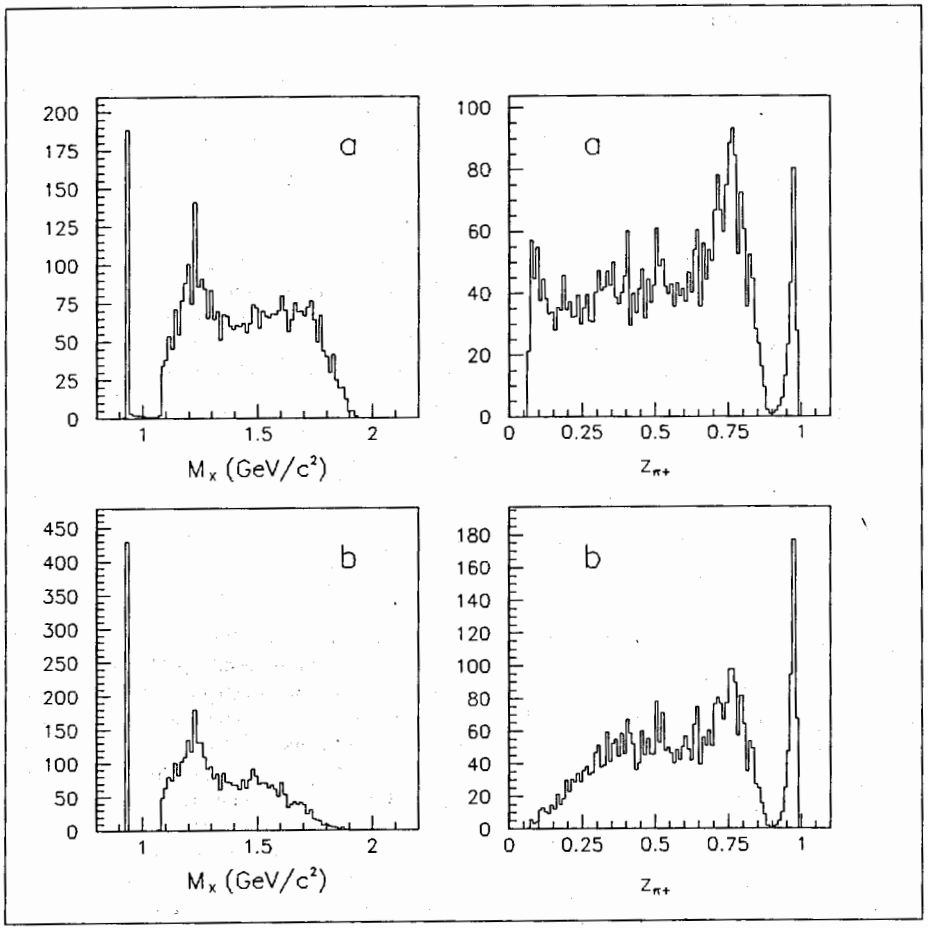

Fig. 16 Missing mass M_x and $z_{\pi+}$ distributions for the reaction $\gamma^V A \to \pi^+ X$ (a) and $\gamma^V D \to \pi^+ X$ (b) at $Q^2 \simeq 1.2$ (GeV/c)^2 and $W \simeq 1.9$ GeV at an angular acceptance $\Delta\Omega_\pi$ for pions. The histograms are normalized to nuclear number; and, for the case of the M_x distribution, we make the shift in nucleon mass.

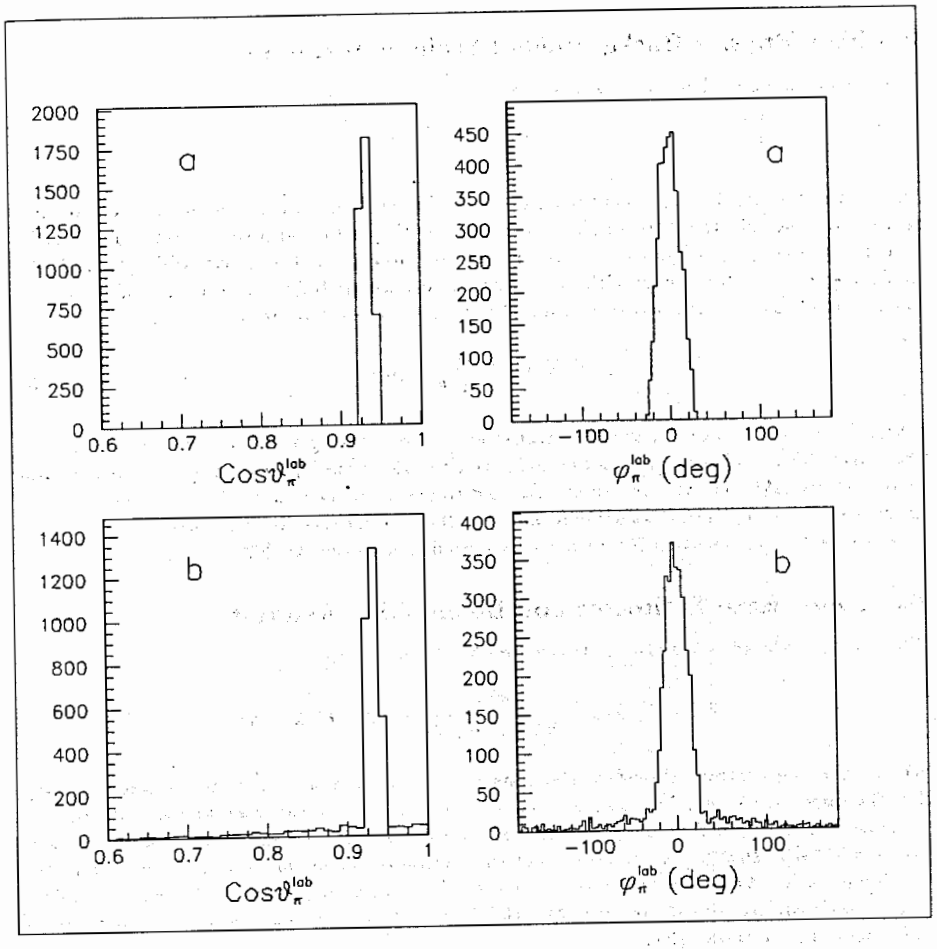

Fig. 17 Distributions for $\cos\vartheta_\pi^{lab}$ and φ_π^{lab} for the reaction $\gamma^V A \to \pi^+ X$ (a) and $\gamma^V D \to \pi^+ X$ (b) at $Q^2 \simeq 1.2$ (GeV/c)^2 and $W \simeq 1.9$ GeV at an angular acceptance $\Delta\Omega_\pi$ for pions. In histograms (b), the pions outside the angular acceptance of the hadron arm, after rescattering in the nucleus, change momentum as well as their direction in flight and are detected in the angular acceptance $\Delta\Omega_\pi$ of the hadron arm. The histograms are normalized to nuclear number.

3.4 Non–Physics Backgrounds (Accidental Rates)

The accidental coincidence rate is given by

$$A = \frac{\tau N_e N_h}{d} \tag{47}$$

where A is the accidental coincidence rate, τ is the resolving time, d is the accelerator duty factor, N_e is the electron arm singles rate and N_h is the hadron arm singles rate. The relative level for accidental coincidences increases with beam intensity and decreases with Q^2, $A \sim N_e N_h$, and N_e and N_h both increase with intensity and decrease with Q^2. An estimate of the singles rates N in each of the spectrometers, may be obtained separately from

$$N = \overline{N}_e \overline{N}_t L \left(\frac{d^3\sigma}{d\Omega dP}\right) \Delta\Omega\Delta P \tag{48}$$

where $\overline{N}_e$ is the number of incident electrons per second on a target, $\overline{N}_t$ is the target density, L is the target thickness, $d^3\sigma/d\Omega dP$ is the inclusive electron scattering or hadron electroproduction cross section, $\Delta\Omega$ and ΔP are the angular and momentum acceptances for the spectrometers. In the electron arm, the cross section formula for the $(e, e'X)$ reaction was used. For the hadron arm we use the cross section for inclusive pion production from Ref.[62].

3.5 Count Rate Estimates and Beam Time Request

The real coincidence count rate is determined by the expression

$$T_{eh} = \overline{N}_e \overline{N}_t L \left(\frac{d^6\sigma}{d\Omega_e dE_e d\Omega_h dP_h}\right) \Delta\Omega_e \Delta E_e \Delta\Omega_h \Delta P_h \tag{49}$$

where $\overline{N}_e$ is the number of incident electrons per second on a target, $\overline{N}_t$ is the target density, L is the target thickness, $\Delta\Omega_e$ and ΔE_e are the electron spectrometer angular and momentum acceptances, $\Delta\Omega_h$ and ΔP_h are the hadron spectrometer angular and momentum acceptances, and $d^6\sigma/d\Omega_e dE_e d\Omega_h dP_h$ is the inclusive hadron electroproduction cross section given in Eq. (18).

Simulated yields for the inclusive $ep \rightarrow e'\pi^+X$ reaction on protons are shown in Table 5. These yields are calculated for $1.0 \leq Q^2$ (GeV/c)$^2 \leq 2.5$ and at $x_B = 0.3$. The length of the cryogenic target cell was 10 cm.

The rationale for the target thickness and beam intensity we plan to implement is based on the expected real to accidental coincidence level.

Listed in Table 6 are the beam time requests needed for a statistical accuracy of $\sim 1\%$ for each target and at each Q^2 point. All targets have areal densities $\rho L = 700$ mg/cm^2. The aggregate amount of beam time is ~ 590 hours. Beam time would be distributed between the targets roughly as: hydrogen target 236 hours, deuterium target 118 hours, calcium target 118 hours, and empty target 118 hours. Taking into account the time we need for spectrometer changes and setups, target changes (nuclear and empty), and other contingency factors, we request a beam time of 700 hours. Expected errors $\sim (2.5)\%$ are presented in Figs. 18 and 19. This type of accuracy will permit us to distinguish between a quark hadronization mechanism and the Glauber model at a confidence level $> 95\%$.

Setup	I_e (μA)	N_e (kHz)	N_π (kHz)	$R_{e\pi}$ (hour^{-1})	$A_{e\pi}$ (hour^{-1})	$R_{e\pi}/A_{e\pi}$ (1ns)	time (hour)
1a	50	48.1	39.1	31129	6759	4.6	8
1b	70	67.3	57.5	61465	13902	4.4	4
2a	90	15.7	79.1	21684	4474	4.8	8
2b	60	10.5	55.0	9407	2074	4.5	17
2c	150	26.2	140.7	71992	13263	5.4	3
3a	150	5.1	140.7	12639	2592	4.9	10
3b	120	4.1	117.0	7838	1725	4.5	16
3c	70	2.4	69.7	2657	600	4.4	45
3d	170	5.8	172.6	19229	3604	5.3	7

Table 5: Yields from the $ep \rightarrow e'\pi^+X$ reaction at $E_0 = 6.0$ GeV and $x_B = 0.30$.

Setup	I_e (μA)	LH_2 $e\pi^+$	LH_2 $e\pi^-$	LD_2 $e\pi^+$	^{40}Ca $e\pi^+$	^{208}Pb $e\pi^+$	Time (hour)
1a	50	8	8	8	8	8	24
1b	70	4	4	4	4	4	12
2a	90	8	8	8	8	8	24
2b	60	17	17	17	17	17	51
2c	150	3	3	3	3	3	9
3a	150	10	10	10	10	10	30
3b	120	16	16	16	16	16	48
3c	70	45	45	45	45	45	135
3d	170	7	7	7	7	7	21

Table 6: Beam time request. Net Beamtime = 590 hours.

3.6 Errors

Because we are measuring *pi*–meson production cross sections, most of the errors will be centered around spectrometer acceptances and efficiencies, luminosities, and radiative corrections. Kinematic errors such as determining θ_e, $\vec{q}$, θ_π, and W should be negligible considering the expected small angular resolutions (0.5 mr horizontal and 1.0 mr vertical) and momentum resolutions (1×10^{-4}) for the HRS2 system in Hall A.

Errors from the other aforementioned components will depend on how well, in the early life of using the HRS2 system, can the errors be resolved from either improvements to hardware, or by analysis techniques, or both. Our expectations for absolute cross section errors run between $2-3\%$; moreover, our goal is to be at the $\sim 2\%$ level — which is not that unlikely, considering that the NE11 group [63] at SLAC have obtained these levels in the past. Also coupled to this way of thinking would be the expected learning curve of understanding the accelerator and the spectrometer components as time progresses at CEBAF. Therefore, the expectation for acheiving the following

$$\left(\frac{\Delta\sigma}{\sigma}\right)_{abs} = \left[0.01^2(lumin.) + 0.01^2(accept.) + 0.01^2(charge) + 0.01^2(rad.corr.)\right]^{1/2} = 2\% \ , \tag{50}$$

is not unrealistic.

Systematic uncertainties resulting from model dependencies from physics backgrounds or multiple scattering contributions have been estimated to be small; furthermore, errors in extracting quantities relating to information about the space–time evolution of hadronization will be dealt with during the off–line analysis period when interpretation of the results is being rendered.

3.7 Data Analysis

From a detailed analysis of π–meson propagation through ^{40}Ca and ^{208}Pb, we propose to make measurements of the nuclear transparency with respect to the different processes of π–meson electroproduction. These are:

1. Transparency with respect to π^+–mesons from the process $ep \rightarrow e'\pi^+ n$;

$$T_{\pi^+ n}(A, Q^2) = \frac{1}{Z}\frac{\sigma\left[eA \rightarrow e'\pi^+ n(A-1)\right]}{\sigma(ep \rightarrow e'\pi^+ n)} \tag{51}$$

   Expected experimental results and theoretical predictions are presented in Fig. 18 for both ^{40}Ca and ^{208}Pb.

2. Nuclear transparency for ^{40}Ca and ^{208}Pb nuclei with respect to π^-–mesons from the process $ep \rightarrow e'\pi^-(\pi^+ p)$ at an off–line missing mass cut $M_x < (m_p + m_\pi)$;

$$T_{\pi^-(\pi^+ p)}(A, Q^2, z) = \frac{1}{A}\frac{d\sigma\{eA \rightarrow e'\pi^-[\pi^+ p(A-1)]\}\,/\,dz}{d\sigma(ep \rightarrow e'\pi^-(\pi^+ p))\,/\,dz} \tag{52}$$

3. Nuclear transparency for ^{40}Ca and ^{208}Pb nuclei with respect to π^+–mesons from the process $ep \rightarrow e'\pi^+(\pi N)$ at an off–line missing mass cut $M_x < (m_N + m_\pi)$;

$$T^p_{\pi^+(\pi N)}(A, Q^2, z) = \frac{1}{A}\frac{d\sigma\{eA \rightarrow e'\pi^+[\pi N(A-1)]\}\,/\,dz}{d\sigma(ep \rightarrow e'\pi^+(\pi N))\,/\,dz} \tag{53}$$

4. Nuclear transparency for ^{40}Ca and ^{208}Pb nuclei with respect to π^+–mesons from the process $ed \rightarrow e'\pi^+(\pi NN)$ at an off–line missing mass cut $M_x < (2m_N + m_\pi)$;

$$T^d_{\pi^+(\pi N)}(A, Q^2, z) = \frac{2}{A}\frac{d\sigma\{eA \rightarrow e'\pi^+[\pi N(A-1)]\}\,/\,dz}{d\sigma(ed \rightarrow e'\pi^+(\pi NN))\,/\,dz} \tag{54}$$

5. Nuclear transparency for ^{40}Ca and ^{208}Pb nuclei with respect to π^+–mesons from the process $ep \rightarrow e'\pi^+ X$

$$T^p_{\pi^+}(A, Q^2, z) = \frac{1}{A}\frac{d\sigma(eA \rightarrow e'\pi^+ X)\,/\,dz}{d\sigma(ep \rightarrow e'\pi^+ X)\,/\,dz} \tag{55}$$

6. Nuclear transparency for ^{40}Ca and ^{208}Pb nuclei with respect to the π^+–mesons from the process $ed \rightarrow e'\pi^+ X$

$$T^d_{\pi^+}(A, Q^2, z) = \frac{2}{A}\frac{d\sigma(eA \rightarrow e'\pi^+ X)\,/\,dz}{d\sigma(ed \rightarrow e'\pi^+ X)\,/\,dz} \tag{56}$$

7. In the end, we will make nuclear transparency measurements with respect to the virtual–photons absorption process;

$$T_{tot}(A, Q^2) = \frac{2}{A}\frac{\sigma^{tot}(eA \rightarrow e'X)}{\sigma^{tot}(ed \rightarrow e'X)} \tag{57}$$

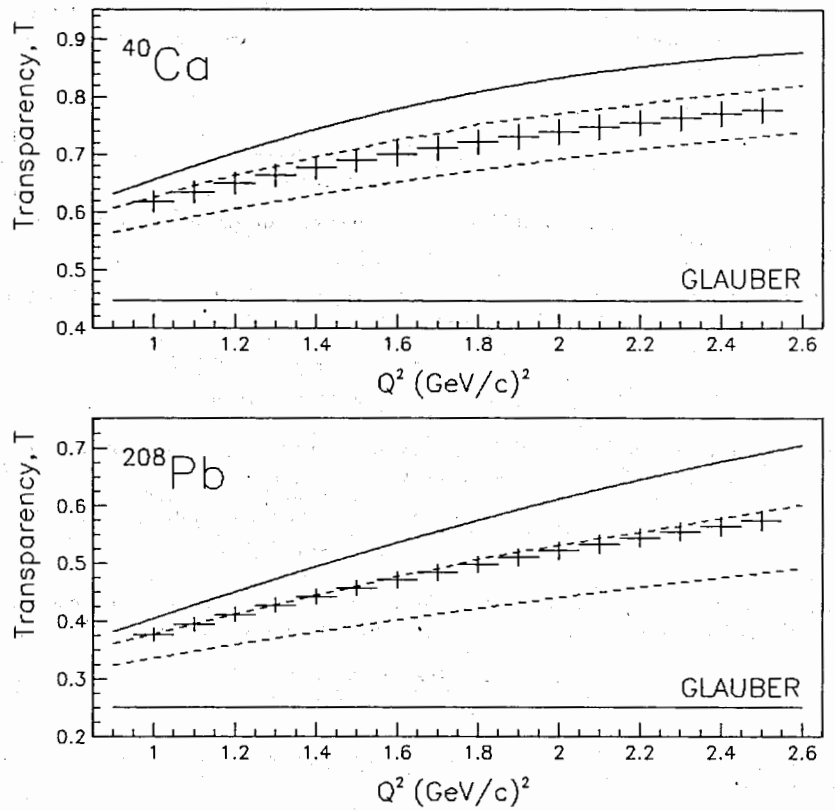

Fig. 18 The Q^2 dependence of the nuclear transparency for ^{40}Ca and ^{208}Pb. Expected errors are show. The curves represent different theoretical models [35,64].

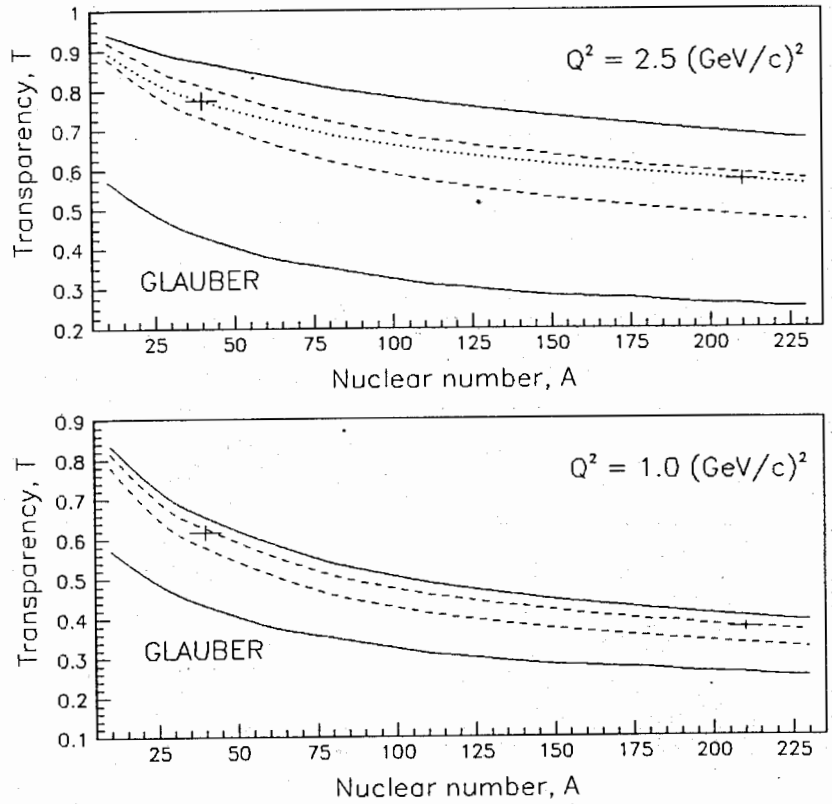

Fig. 19 The A dependence of the nuclear transparency at high [Q^2 = 2.5 (GeV/c)^2] and low [Q^2 = 1.0 (GeV/c)^2] values of Q^2 for the proposed experiment. The expected experimental results for ^{40}Ca and ^{208}Pb nuclei are presented. The curves represent different theoretical models [35,64].

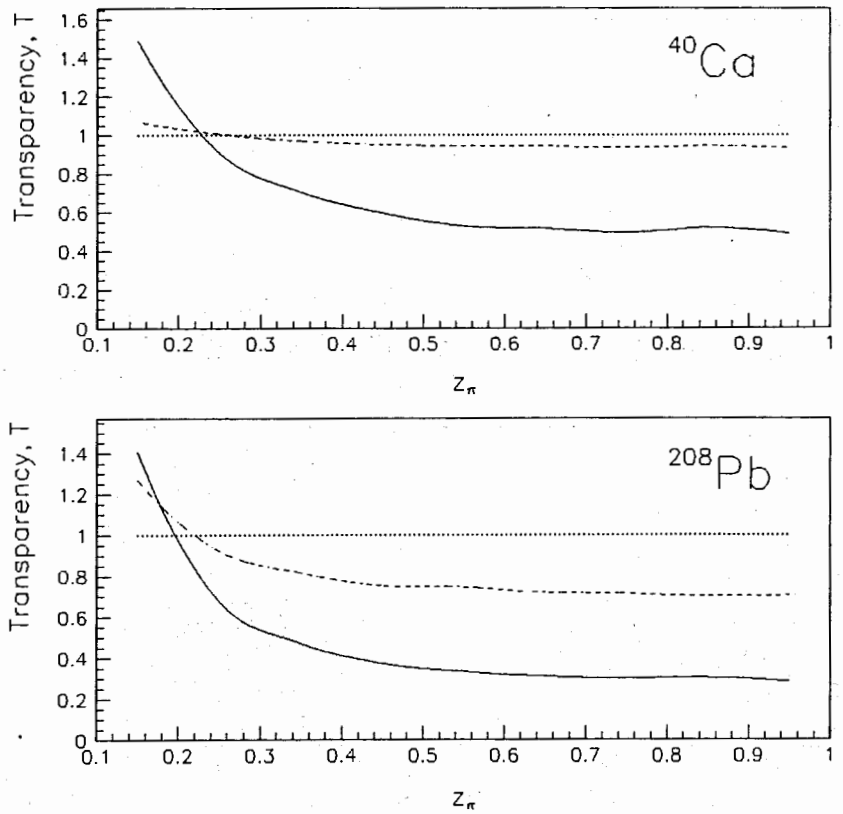

Fig. 20 The z_π dependence of the nuclear transparency for ^{40}Ca and ^{208}Pb nuclei. Solid curves: formation time $\tau_F = 0$ (Glauber), dashed curves: $\tau_F = 5$ fm.

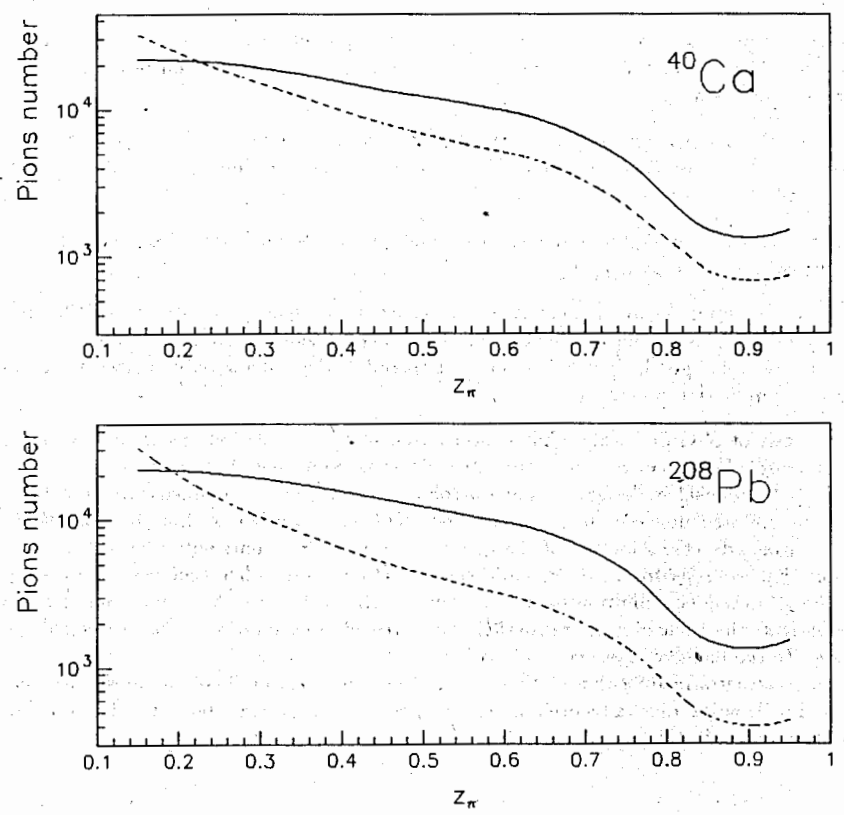

Fig. 21 Pion yields vs. z_π at formation time $\tau_F = 0$ (Glauber). Solid curves: pion yields from a single nucleon; dashed curves: pions yields from a nucleus (after rescattering) normalized to nuclear number A.

3.8. Summary

This experiment plans to show that there is a space–time characterization for quark hadronization processes. If we extract a space–time structure for a quark hadronization process, we can then perform the following:

1. A detailed investigation for transparency of nuclear matter to the electroproduction of π^+–mesons and the determination of its dependence on the kinematic variables ν, Q^2, E_{π^+}, and z.

2. Extraction of the quark interaction cross section σ_q with internuclear nucleons and examine its dependence on ν and Q^2.

3. Finally, obtaining the most adequate explanation for the space–time structure of hadron leptoproduction is the most salient point of this experiment. Included here would be explanations on the fast hadron formation time τ_F and its dependence on kinematic variables for leptoproduction processes.

Our analysis of physics backgrounds concentrated only on contributions from resonances and rescattering effects because these are the most important contributions in the region of kinematics this proposal is designed. The outcome of these analyses demonstrate that these contributions are well understood and controlled. Of course during off–line analysis of the data, we can include Fermi motion of the intranucleus nucleons, contributions from coherent production of ρ^0–mesons from nuclei, radiative corrections, and other processes. Moreover, because the ρ^0–meson contribution to the inclusive spectra of $\pi^\pm$–mesons is not small, we will try to investigate the nuclear color transparency with respect to the process $\gamma^V p \to \rho^0 p$ [65] and its influence to the inclusive spectra of π^+–mesons.

The analysis performed in this section reveals that the goals of this experiment are very realistic and will lead to more advanced discernment concerning strong interaction dynamics for the transition region in Q^2.

4. Conclusion

Based on the PAC 7 recommendation that we should envision performing this experiment at a beam energy of 6 GeV to ensure hard virtual photon–quark scattering, we feel that with a firm understanding of the physics issues and the use of a superb HRS spectrometer system in Hall A and the CW beam at CEBAF, that our goals can be met with high expectations. Also, the 6 GeV beam allows us to examine larger values of W with a wider range in Q^2. This kinematic flexibility allows us to perform a detailed analysis on the dependence of the hadronization parameters τ_F and σ_q on the kinematic variables of the virtual photon and the final pion.

We would like to once again emphasize that this document was proposed to investigate two very similar, but yet very different phenomena: nuclear color transparency and quark–hadronization mechanisms. In the first case the virtual photon is absorbed by the colorless pion as a whole via the reaction $\gamma^V p \to \pi^+ n$ and then the "small–sized pion" propagates through it's nuclear environment. In the second case, we have a very different picture: the virtual photon is absorbed by the color–quark state and then the quark during its QCD evolution inclusively transforms to colorless pions. Of course in this case $z \leq (0.8 - 0.9)$, the pions do not possess such a high momentum as from the reaction $\gamma^V p \to \pi^+ n$ where $z \simeq 1.0$. The existence or absence of one of these two phenomena are not connected with the existence or the absence, respectively, of the other phenomenon. For this reason, these two phenomena need to be treated and investigated as different physical phenomena; and of course, the formation times τ_F^{color} and τ_F^{hadro} for these two different phenomena, need to be considered as a different and distinct values.

Other CEBAF projects that have been proposed want to study quark hadronization mechanisms with a measurement of the process $\gamma^V p \to \pi^+ n$. As we note above, these experiments can only obtain information about the nuclear color transparency but not about quark hadronization mechanisms. To obtain information about the latter, we need to make measurements in wider regions of z; that is, $0.6 \leq z \leq 1.0$ as we propose to do in this project.

References

[1] F. A. Berends, Phys. Rev. **D1**, 2590 (1970).

[2] R. C. E. Devenish, D. H. Lyth, Phys. Rev. **D5**, 47 (1972).

[3] F. Gutbrod, G. Kramer, Nucl. Phys. **B49**, 461 (1972).

[4] C. J. Bebek *et al.*, Phys. Rev. **D17**, 1693 (1976).

[5] P. Brauel *et al.*, Z. Phys. **C3**, 101 (1979).

[6] C. N. Brown *et al.*, Phys. Rev. **D8**, 92 (1973).

[7] C. J. Bebek *et al.*, Phys. Rev. Lett. **37**, 1326 (1976).

[8] C. J. Bebek *et al.*, Phys. Rev. **D13**, 25 (1976).

[9] C. J. Bebek *et al.*, Phys. Rev. **D9**, 1229 (1974).

[10] P. Joos *et al.*, Nucl. Phys. **B113**, 53 (1976).

[11] K. Wacker *et al.*, Nucl. Phys. **B144**, 269 (1978).

[12] Ch. Berger *et al.*, Phys. Lett. **B70**, 471 (1977).

[13] A. Sofair *et al.*, Nucl. Phys. **B42**, 369 (1972).

[14] J. M. Scarr *et al.*, Nucl. Phys. **B135**, 224 (1978).

[15] J. C. Alder *et al.*, Nucl. Phys. **B46**, 415 (1972).

[16] J. M. Scarr *et al.*, Nucl. Phys. **B135**, 224 (1978).

[17] R. G. Badalian, Yad. Fiz. **50**, 1120 (1989) and Sov. J. Nucl. Phys. **50**(4), 698 (1989).

[18] J. Franz *et al.*, Preprint DESY 81-023, Hamburg, 1981.

[19] G. Miller *et al.*, Phys. Rev. **D5**, 528 (1972).

[20] F. W. Brasse *et al.*, Nucl. Phys. **B110**, 413 (1976).

[21] F. W. Brasse *et al.*, Nucl. Phys. **B39**, 421 (1972).

[22] R. D. Field, R. P. Feynman, Nucl. Phys. **B136**, 1 (1978).

[23] E. Reya, Phys. Rep. **69C**, 195 (1981).

[24] K. Huang, *Quarks, Leptons and Gauge Fields*, World Scientific, Singapore, 1982.

[25] P. Allen *et al.*, Nucl. Phys. **B214**, 369 (1983).

[26] V. R. O'Dell *et al.*, Phys. Rev. **D36**, 1 (1987).

[27] R. J. Apsimon *et al.*, Z. Phys. **C47**, 397 (1990).

[28] K. Berkelman, Proc. XVI Int. Conf. on High Energy Physics, Batavia, Illinois, **v.4**, 41 (1972).

[29] J. F. Martin *et al.*, Phys. Lett. **B65**, 483 (1976).

[30] P. Joos *et al.*, Nucl. Phys. **B122**, 365 (1977).

[31] C. K. Chen *et al.*, Nucl. Phys. **B133**, 13 (1978).

[32] S. J. Brodsky, A. H. Mueller, Phys. Lett. **B206**, 685 (1988).

[33] G. R. Farrar *et al.*, Phys. Rev. Lett. **61**, 686 (1988).

[34] A. Bialas, T. Chmaj, Phys. Lett. **B133**, 241 (1983).

[35] R. G. Badalian, Z. Phys. **C55**, 647 (1992); Preprint YERPHI-1305(91)-90, Yerevan, 1990.

[36] R. Glauber, Usp. Fiz. Nauk **103**, 641 (1971).

[37] V. N. Gribov, Proc. VIII Winter School LINP, Leningrad, 1973, p.5.

[38] J. D. Bjorken, *Hadron final states in deep inelastic processes*, in Current induced reactions. Proc. Int. summer Institute on Theoretical Particle Physics, p.93, Hamburg, 1975.

[39] N. N. Nikolaev, Usp. Fiz. Nauk **134**, 369 (1981).

[40] Ya. I. Azimov *et al.*, Proc. XVII Winter School LINP, Leningrad, 1982, p.162.

[41] L. V. Gribov *et al.*, Proc. XXII Winter School LINP, Leningrad, 1987, p.61.

[42] N. N. Badalian, R. G. Badalian, Z. Phys. **C48**, 587 (1990).

[43] T. H. Bauer *et al.*, Rev. Mod. Phys. **50**, 261 (1978).

[44] Reviev of Particle Properties, Phys. Rev. **D45**, (1992).

[45] J. Ashman *et al.*, Phys. Lett. **B202**, 603 (1988).

[46] M. Arneodo *et al.*, Phys. Lett. **B211**, 493 (1988).

[47] V. S. Barashenkov, V. D. Toneev, Interaction of high energy particles and atomic nuclei with nuclei, Moscow, Atomizdat, (1972).

[48] N. W. Bertini *et al.*, Phys. Rev. **C9**, 522 (1974).

[49] N. W. Bertini *et al.*, Phys. Rev. **C14**, 590 (1976).

[50] J. P. Bondorf *et al.*, Phys. Lett. **B65**, 217 (1976).

[51] J. P. Bondorf *et al.*, Z. Phys. **A279**, 385 (1976).

[52] V. D. Toneev, K. K. Gudima, Nucl. Phys. **A400**, 173 (1983).

[53] O. Kofoed-Hansen, Nucl. Phys., **B54**, 42 (1973).

[54] G. B. Alaverdian, A. V. Tarasev, V. V. Uzhinskii, Sov. J. Nucl. Phys., **25**, 666 (1977).

[55] G. B. Alaverdian *et al.*, Sov. J. Nucl. Phys., **31**, 776 (1980).

[56] L. S. Osborne *et al.*, Phys. Rev. Lett. **40**, 1624 (1978).

[57] A. Arvidson *et al.*, Nucl. Phys. **B246**, 381 (1984).

[58] D. S. Baranov *et al.*, Yad. Fiz. **40**, 1454 (1984).

[59] Reviev of Particle Properties, Phys. Rev. **D50**, (1994).

[60] *CEBAF Conceptual Design Report*, Newport News, Virginia (April 1990).

[61] N. N. Badalian, R. G. Badalian, H. R. Gulkanyan, Yad. Fiz. **46**, 1759 (1987) and Sov. J. Nucl. Phys. **46**(6), 1052 (1987).

[62] J. W. Lightbody and J. S. O'Connell, Comp. In Phys., May/June (1988) 57.

[63] P. E. Bosted *et al.*, Phys. Rev. Lett. **68**, 3841 (1992).

[64] R. G. Badalian, Phys. Lett. **B296**, 440 (1992).

[65] M. Arneodo *et al.*, Preprint CERN-PPE/94-146, (1994).

Received by Publishing Department
on December 29, 1994.

Бадалян Н.Н. и др. E1-94-519
Электророждение заряженных пионов на ^{1}H, ^{2}H, ^{40}Ca и ^{208}Pb

В процессах глубоконеупругого рассеяния лептонов при $Q^2 >> m_c^2$, где $m_c \cong m_Q \approx 0{,}3$ ГэВ, m_Q — масса аддитивного кварка, виртуальный фотон передает кварку всю свою энергию ν в течение временного интервала $\tau_P \cong \nu/Q^2$. В соответствии с КХД сечение такого процесса $\sim 1/Q^2$, более того, к моменту $\tau_F \cong \nu/m_c^2 >> \tau_P$ точечноподобная кварковая система должна превращаться в адроны нормальных размеров. В течение временного интервала $\tau_P < t < \tau_F$ такая точечноподобная кварковая или кварк-глюонная система взаимодействует с ядерным веществом с малым сечением, что приводит к увеличению выхода адронов (например, π^+-мезонов) на ядрах по сравнению со случаем, когда адроны формируются в точке взаимодействия виртуального фотона с кварком. Такой протяженный механизм адронизации кварков может быть исследован при энергиях начальных электронов 6 ГэВ, которое может быть достигнуто на ускорителе СЕБАФ.

В работе предлагается измерить инклюзивные спектры электророждения $\pi^{\pm}$-мезонов на ^{1}H, а также π^+-мезонов на ^{2}H, ^{40}Ca и ^{208}Pb в процессах $(e,e'\pi^{\pm})$ при 1 ГэВ$^2 \le Q^2 \le 2{,}5$ ГэВ^2, $W \ge 1{,}92$ ГэВ и $x_B = 0{,}3$ в зале А на ускорителе СЕБАФ. Показано, что из анализа Q^2-зависимости прозрачности ядерного вещества мы можем получить информацию относительно пространственно-временных масштабах процесса адронизации кварков.

Работа выполнена в Лаборатории высоких энергий ОИЯИ.

Сообщение Объединенного института ядерных исследований. Дубна, 1994

Badalian N.N. et al. E1-94-519
Electroproduction of Charged Pions from ^{1}H, ^{2}H, ^{40}Ca and ^{208}Pb

In deep-inelastic scattering at squared four-momentum transfers $Q^2 >> m_c^2$, where the mass m_Q of the additive quark is $m_c \cong m_Q \approx 0{,}3$ GeV, the virtual photon can transfer its energy to the quark during a time interval $\tau_P \cong \nu/Q^2$. With respect to perturbative QCD, the cross section for this process is $\sim 1/Q^2$; moreover, during the time interval $\tau_F \cong \nu/m_c^2 >> \tau_P$, the point-like configuration *must* transform into a normal-sized hadron. Between the time interval $\tau_P < t < \tau_F$, this point-like quark or quark-gluon configuration can interact with nuclear matter with only small cross section. Such a delayed hadronization mechanism will increase the yield of hadrons (in particular, π^+-mesons) relative to the case when hadron production can take place at the virtual-photon quark interaction point. This hadronization process can be studied at energies available after the first energy upgrade at CEBAF; namely, at a beam energy of 6.0 GeV.

We propose to measure in Hall A the inclusive electroproduction of $\pi^{\pm}$-mesons on ^{1}H and π^+-mesons on ^{2}H, ^{40}Ca, and ^{208}Pb utilizing the $(e,e'\pi^{\pm})$ reaction for $1.0 \le Q^2$ (GeV/c)$^2 \le 2.5$, at an invariant energy $W > 1.92$ GeV, and at $x_B = 0.3$. From a Q^2-dependent analysis of the nuclear matter transparency, we can extract information about the space-time scale for the mechanism of quark hadronization.

The investigation has been performed at the Laboratory of High Energies, JINR.

Communication of the Joint Institute for Nuclear Research. Dubna, 1994